Representation of Tropical Indian Ocean in CFSv2 and the possible impacts on the monsoon teleconnections

C. Gnanaseelan and Jasti Chowdary

G. Srinivas, Anant Parekh, Rashmi Kakatkar, Darshana Patekar

Outline

Biases in CFSv2 with emphasis on TIO subsurface

Representation of ENSO response in CFSv2

Non ENSO teleconnection in CFSv2

Surface and subsurface biases

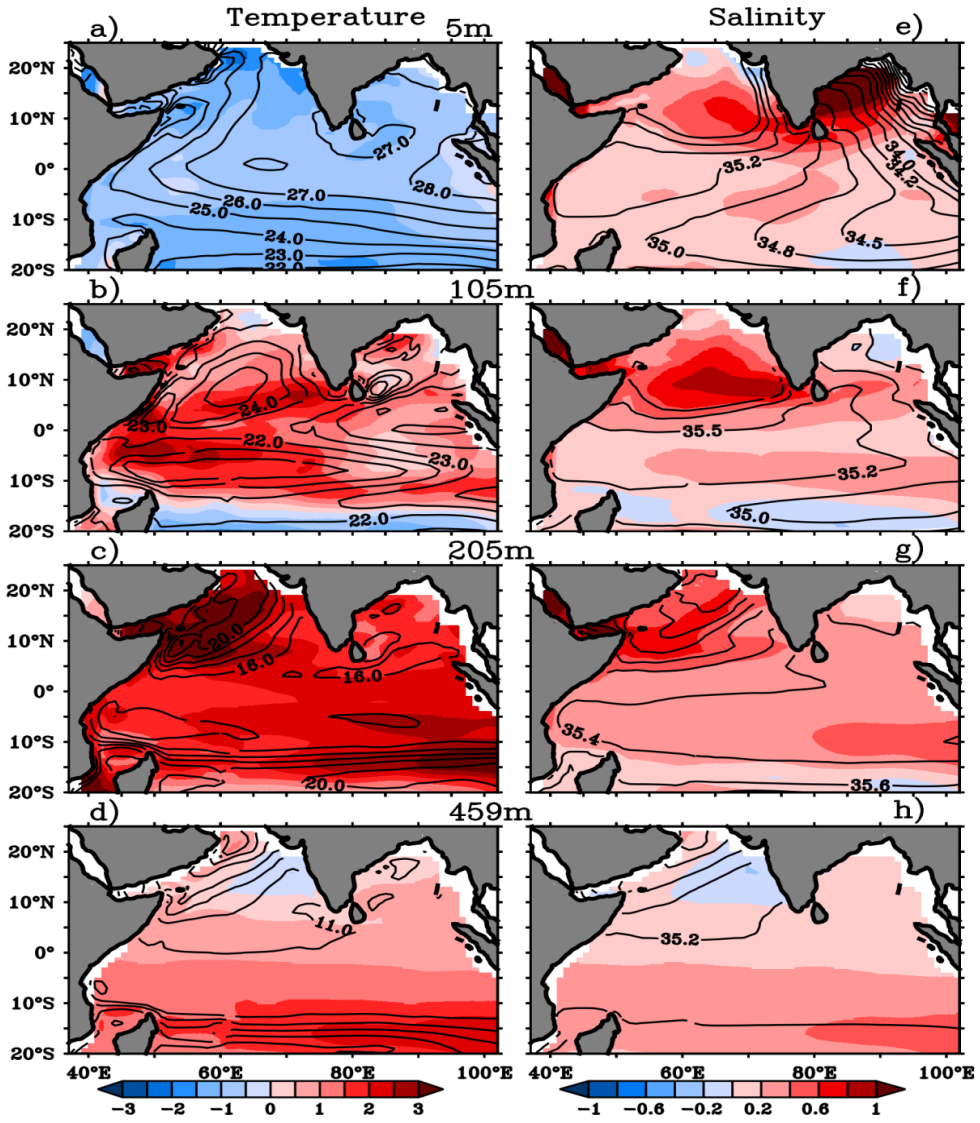

CFSv2 annual mean temperature (contours; °C) and bias (shaded; °C) at different depths (a) 5m, (b) 105m, (c) 205m and (d) 459m over the TIO region and (e)-(h) is same as (a)-(d) but for salinity (psu). Bias is calculated as difference between CFSv2 and WOA13.

✓In addition to the surface cold bias, strong warm bias below the thermocline is apparent in CFSv2. Subsurface temperature bias in CFSv2 is more than 3°C over the WEIO, AS and southeast TIO regions.

✓On the other hand, surface salinity bias is positive in the entire TIO region with maximum being located over Bay of Bengal. Excessive evaporation rather than insufficient precipitation in CFSv2 is mainly responsible for positive surface salinity bias over the TIO (Parekh et al. 2015; Chowdary et al. 2016 Oceanography).

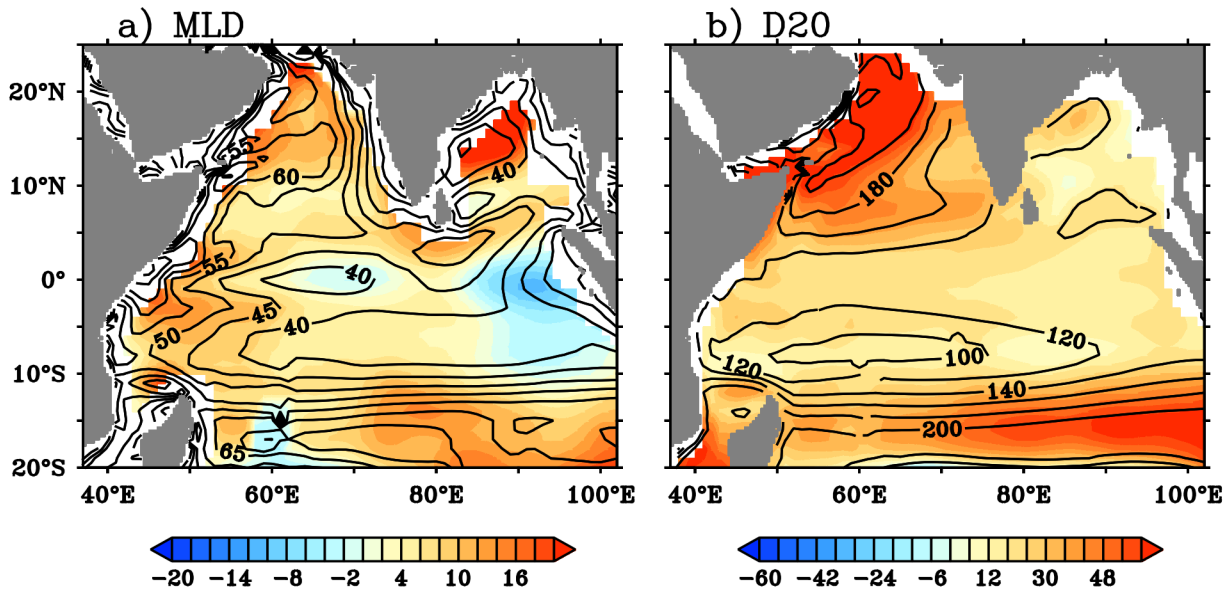

CFSv2 annual mean mixed layer depth (contour; m) and bias (shaded; m) and (b) mean Thermocline (D20, 20°C isotherm) depth (contour; m) and bias (shaded; m). Biases are calculated with respect to WOA13.

Annual mean spatial distribution of MLD reveals the existence of deeper MLD in CFSv2 as compared to observations in the TIO except over the eastern and central equatorial IO.

CFSv2 also displays strong positive bias in thermocline depth (D20) over the Arabian Sea and southern TIO.

These deep MLD and D20 in the model indicate misrepresentation of vertical thermal structure and mixing in CFSv2.

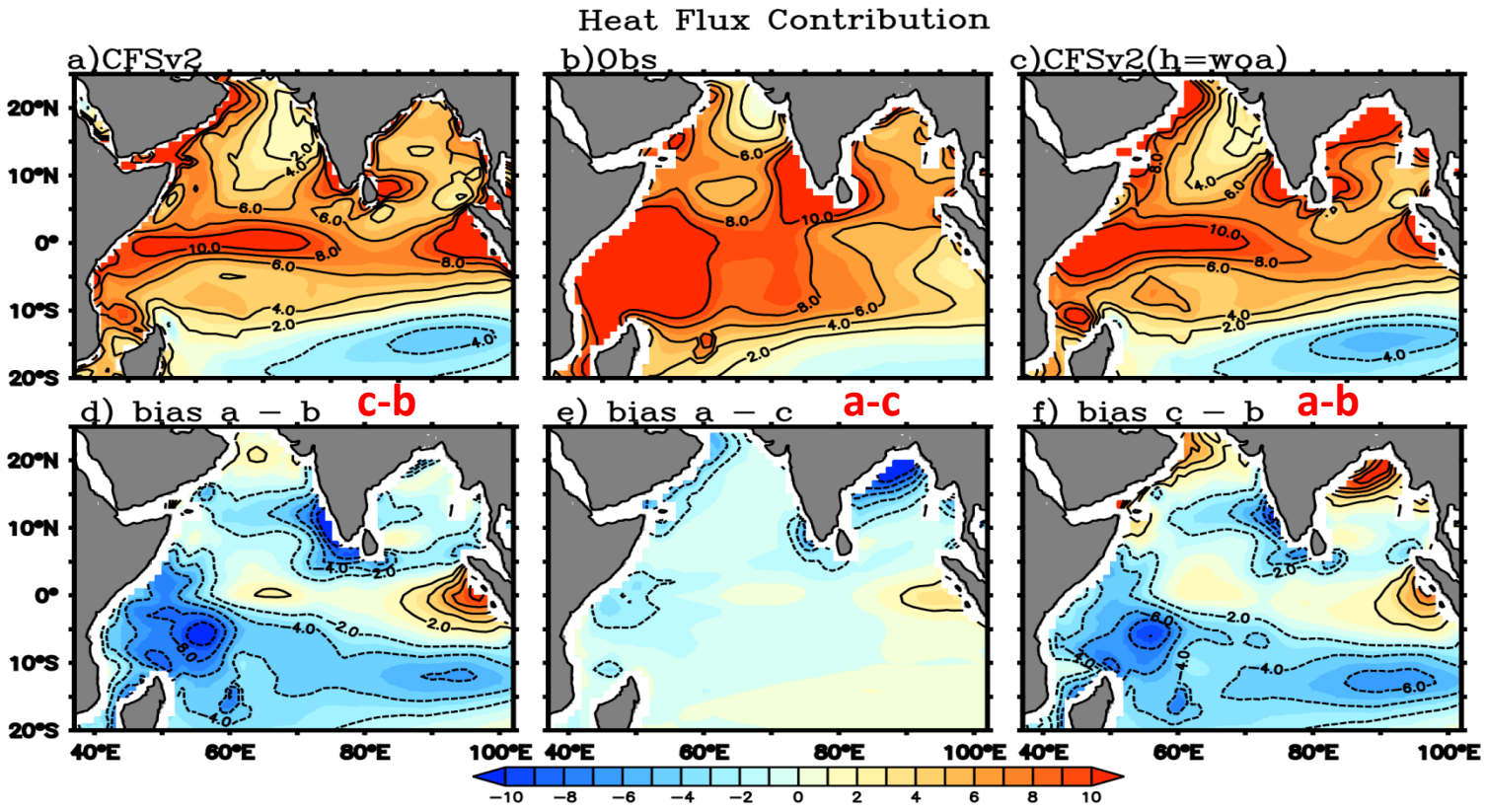

$Q_{net}/(\rho c_p h)$

Contribution of net heat flux to mixed layer temperature (CFSv2 $Q_{net/}\rho c_p h$) where mixed layer depth (*h)* is considered from CFSv2, (b) same as in (a) but Qnet from Tropflux and *h* from WOA13, and (c) same as in (a) but Qnet is from CFSv2 and *h* is from WOA13. (d) Heat flux (Qnet) only contribution to SST bias which is (c) minus (b), (e) contribution of mixed layer depth which is (a) minus (c), and (f) contribution of heat flux and *h* ($Q_{net/}\rho c_p h$) which is (a) minus (b). Units are °C.

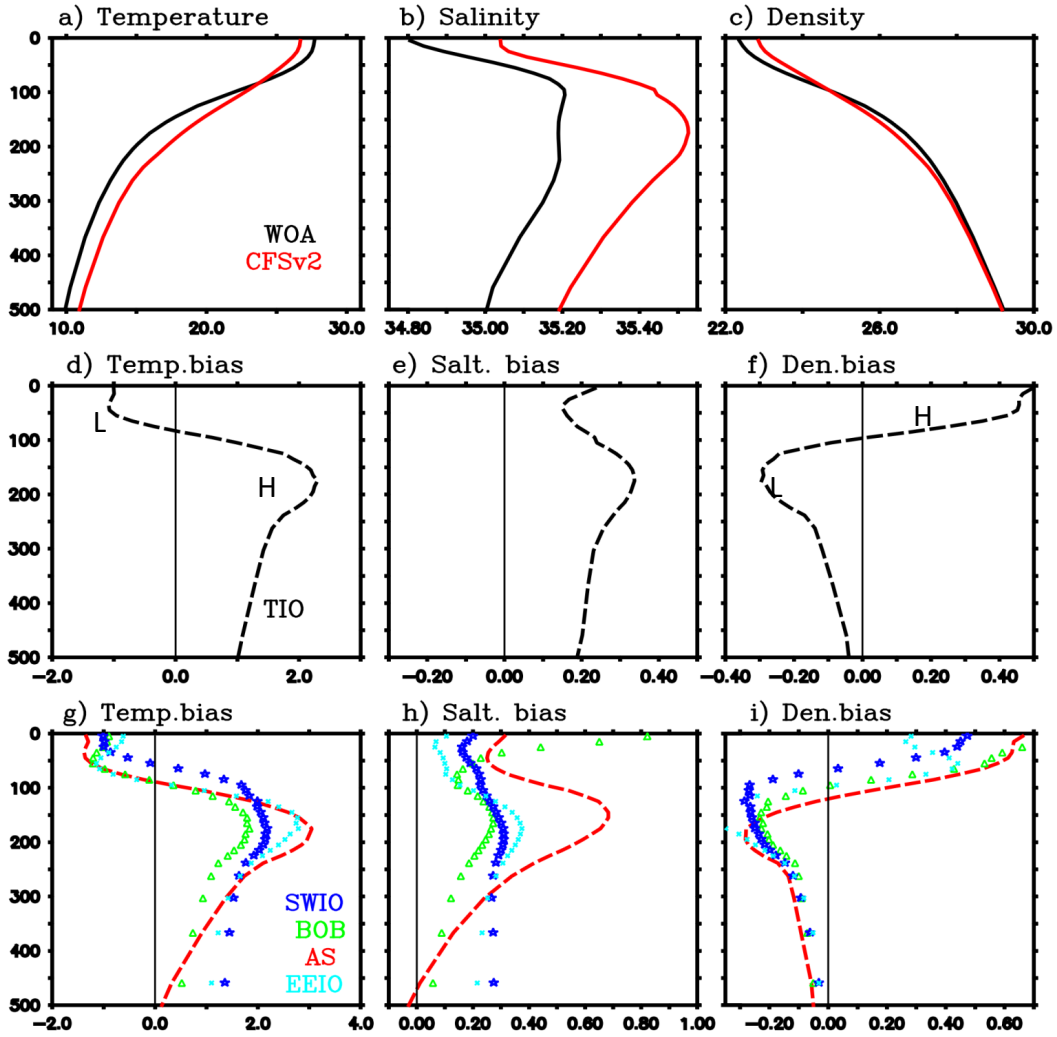

Vertical profiles in upper 500m [Annual mean area averaged in the TIO region (40°E-100°E; 20°S-20°N)] for CFSv2, and WOA13. (a) Temperature (°C), (b) Salinity (psu) and (c) Density (kg m^{-3}) and (d)-(f) same as (a)-(c) but for bias. (g) –(i) are same as (d)-(f) but for different regions of TIO.

✓***Vertical profiles* reveals *persistent cold bias of up to 1°C in the upper 80m in CFSv2 (Fig. 3d) and warm subsurface bias exceeding 2°C around 175m, which is consistent with the spatial temperature bias.***

✓***Such large TIO subsurface temperatures and salinity biases in CFSv2 affect the vertical density structure (Fig. c). In fact, the model density indicates positive biases in the upper 100m and negative biases below that, as compared to WOA13.***

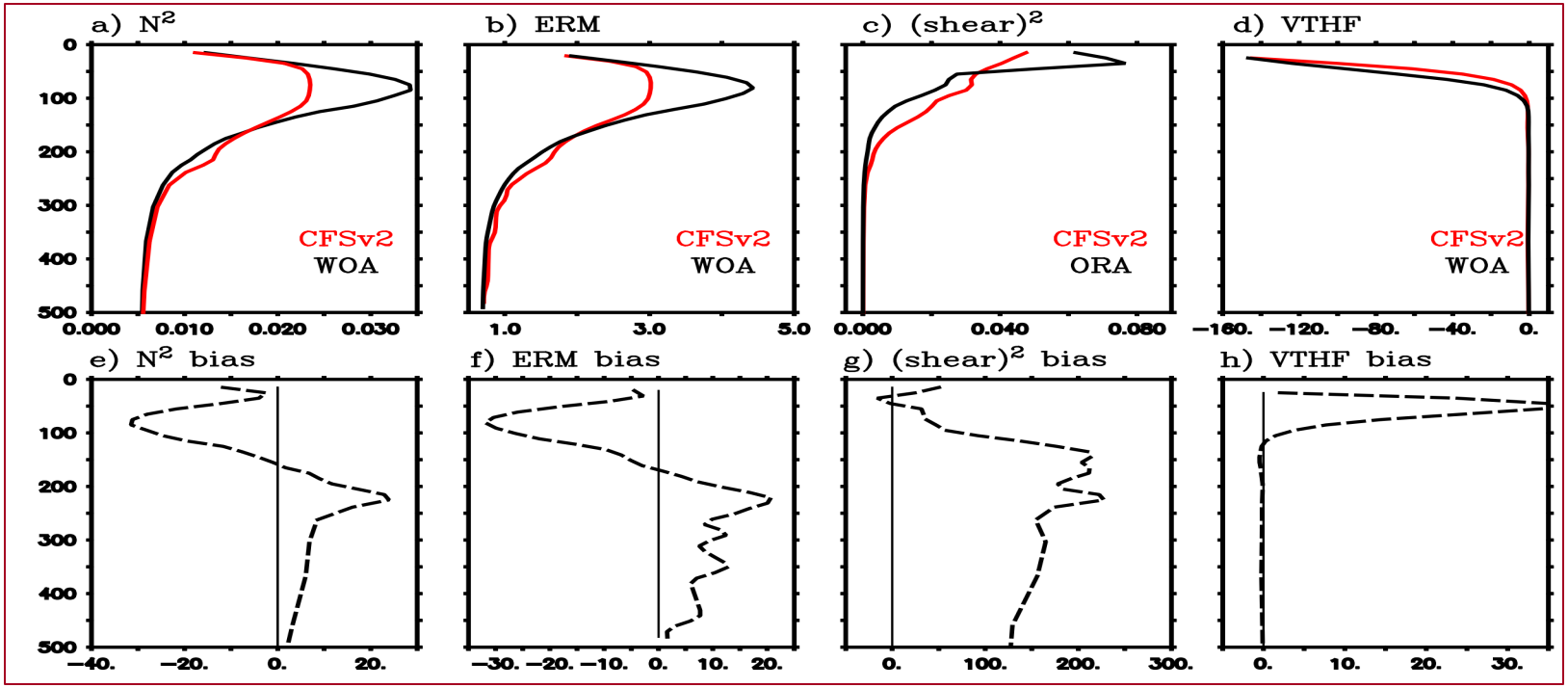

Vertical profiles of (a) Brunt-Vaisala frequency (N^2; 10^{-2} s^{-2}), (b) ERM (Jm^{-2}), (c) square of the vertical shear of horizontal currents (10^{-4} s^{-2}) and (d) vertical turbulent heat flux (Wm^{-2}). (e) – (h) are same as (a) – (d) but for bias. Bias in N^2 profiles and ERM of CFSv2 are calculated with respect to WOA13. In case of vertical shear CFSv2 bias is calculated with respect to ORAS4. Vertical turbulent heat flux bias is with respect to WOA13/MOM5. Note that biases are normalized with respect to observations and presented in percentage except for Vertical turbulent heat flux.

✓The stability (Brunt-Vaisala frequency; N^2) is relatively weaker in CFSv2 for the upper 150m than the observed, which is apparent in the bias (Fig. e). On the other hand, stability is higher than WOA13 below 200m in CFSv2.

✓It is evident that the ERM is underestimated in CFSv2 by up to 30% especially in 30 to 175m depth.

Contribution of advection through eastern (at 100°E) and southern (20°S) boundaries to TIO temperature

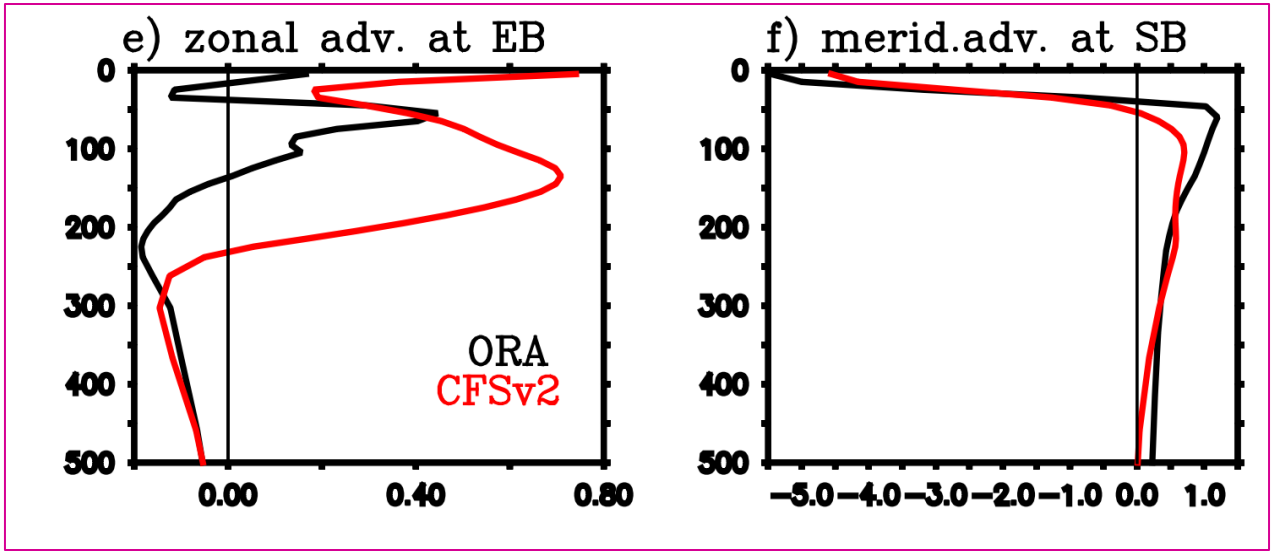

✓Contribution of zonal advection at eastern boundary is up to 0.7°C/s (maximum at 150m) in CFSv2 and 0.4°C/s (maximum at 50m) in ORAS4. Meridional advection through the southern boundary is consistent with ORAS4.

✓ Actual TIO subsurface temperature bias is about three times of ITF contribution. Therefore the subsurface warm bias is mainly caused by excess vertical shear of horizontal currents induced downward transfer of heat.

To Summarize.....

✓**The strong vertical shear in horizontal currents in the model paves the way for a deeper penetration of the warm waters, resulting in the subsurface warm bias.**

✓**Corroborated by anomalously strong vertical shear with surface cold and subsurface warm bias, the underestimated upper ocean stratification in CFSv2 is further feedback to subsurface warm bias.**

✓ **These processes favour enhanced mixing of warm surface water with subsurface. Apart from this, excess Indonesian throughflow warm water partly contributes to the southern TIO subsurface temperature bias.**

Association between mean and interannual equatorial Indian Ocean subsurface temperature bias in a coupled model (CFSv2) hindcast

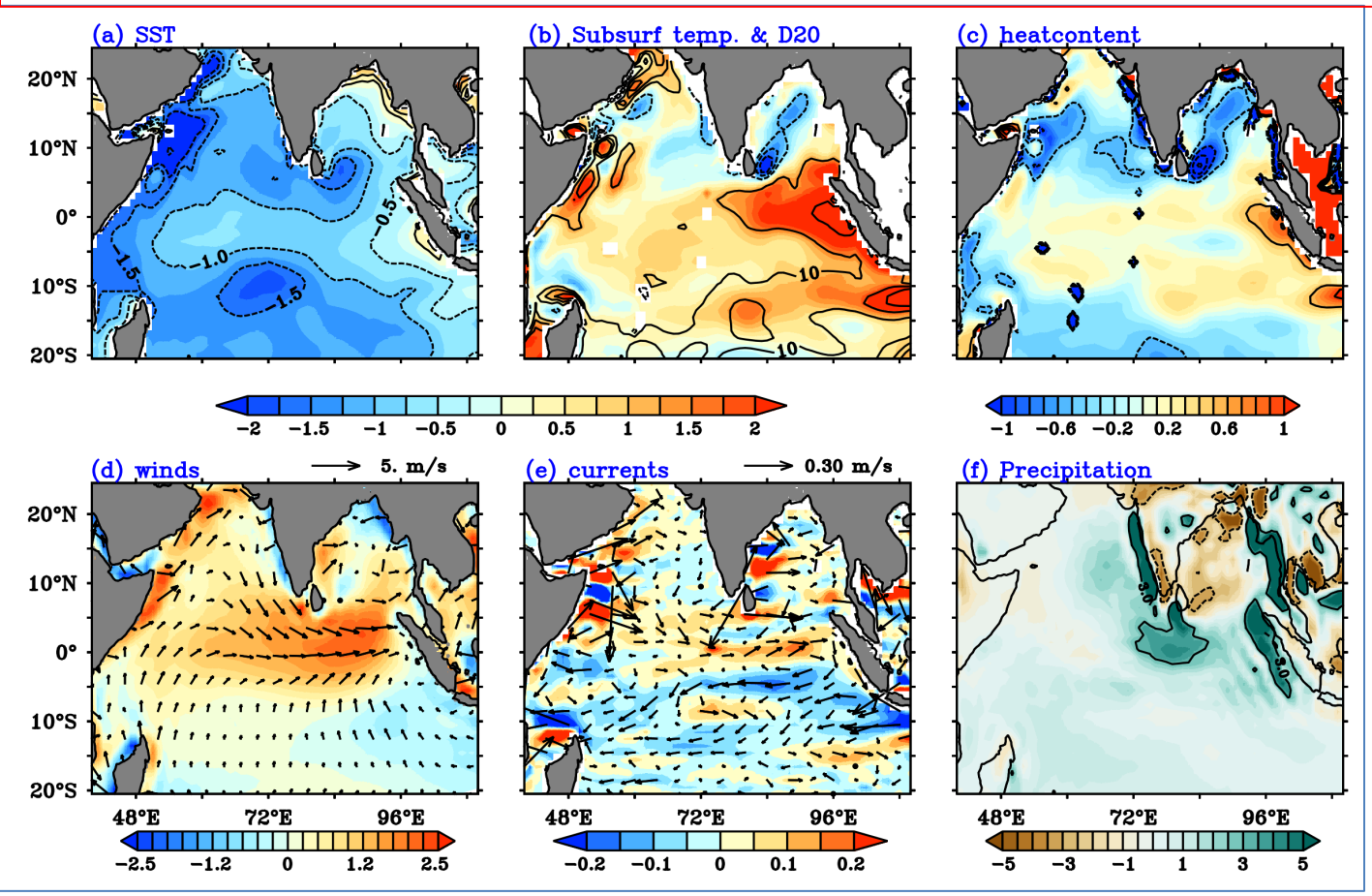

JJAS mean bias

Srinivas et. al. 2018
Climate Dynamics

(a) SST (shaded and contour; ^{o}C) and (b) subsurface temperature averaged over a depth of 120 -140 m (shaded; ^{o}C) and thermocline depth (D20, contour; m), and (c) heat content of upper 150 m depth (shaded and contour; ^{o}C), (d) surface winds (vectors; m/s) and zonal wind component (shaded; m/s), (e) surface currents (vectors; m/s) and zonal current (shaded; m/s) averaged over upper 50 m depth and (f) precipitation (shaded and contour; mm/day). Bias is calculated as difference between CFSv2 and HadI, ERA-Interim winds, ECCO2 currents and CMAP precipitation.

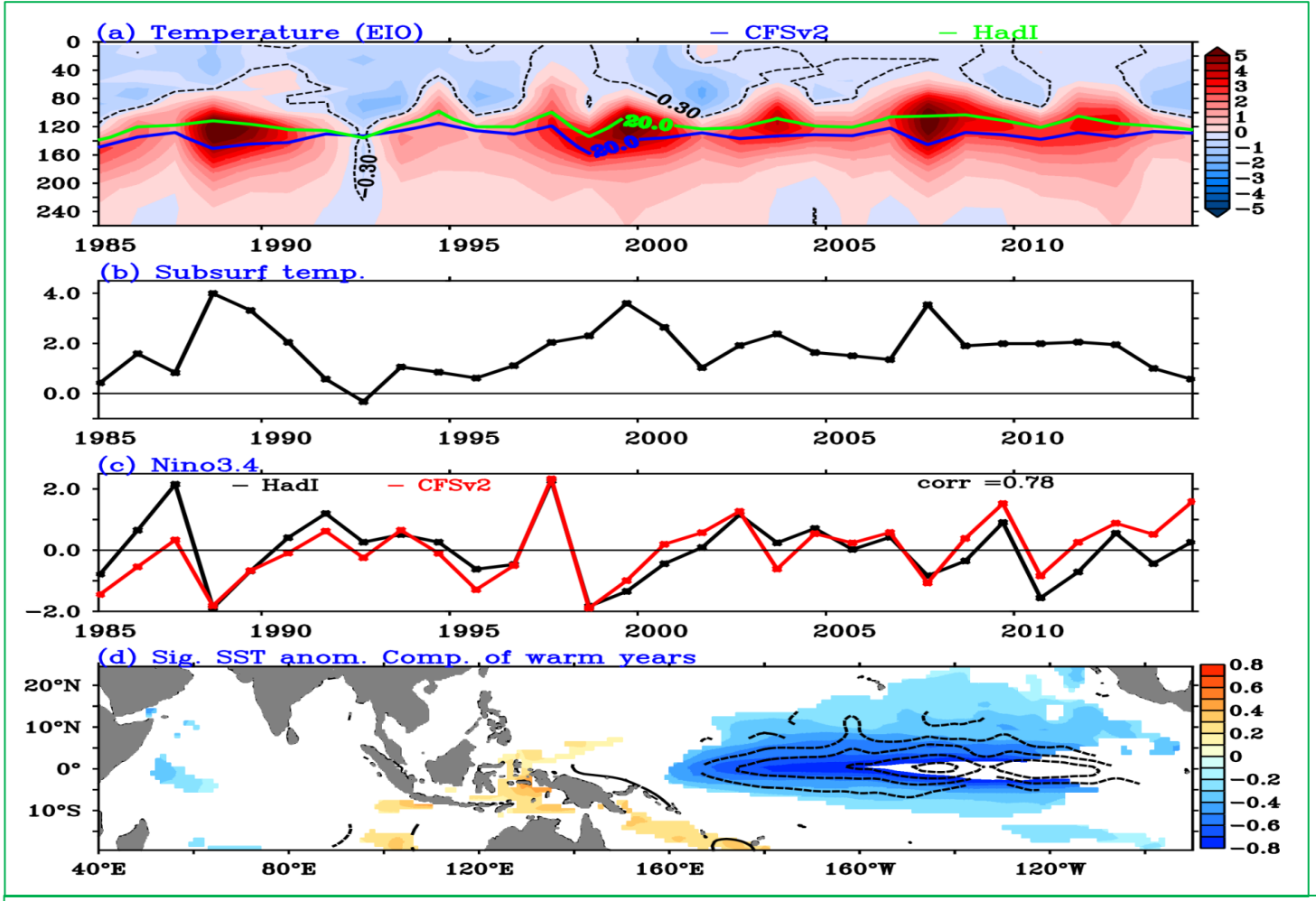

Srinivas et. al. 2018
Climate Dynamics

(a) Depth – Time plot of (JJAS) temperature bias averaged over EIO (90°E to 100°E and 5°S to 5°N) (shaded and contour; °C) and 20°C isotherm (contour; CFSv2 blue line and HadI Green line) (b) time series of subsurface temperature bias (average for 120 – 140 m; °C) over EEIO, (c) time series of CFSv2 Nino 3.4 region SST anomalies (black line) and DMI (red line; °C) and (d) warm year composite of SST anomalies (CFSv2 (shaded) and HadI EN4 product (contours); °C) significant at 90% confidence level is displayed. Bias is calculated with respect to HadI.

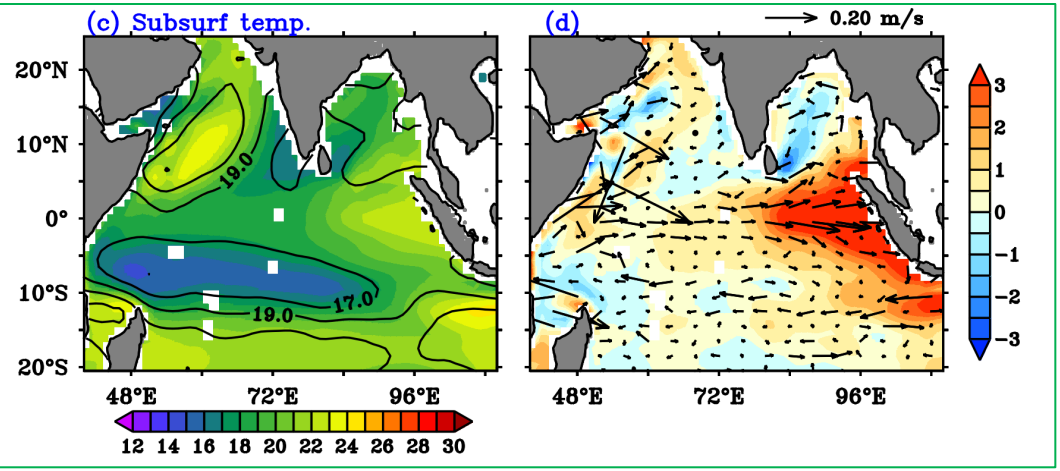

Composite of strong warm (JJAS) years : (c) subsurface temperature (average of 120 -140 m) (CFSv2 (shaded) and HadI EN4 (contour); ºC) and (d) bias in subsurface temperature (shaded; ºC) and currents averaged over same depth (vectors; m/s).

Subsurface temperature bias (ºC) averaged over 5°S to 5°N and 120 – 140 m depth for (a) annual mean (black line) and La Niña composite or maximum bias years (red line) during summer.

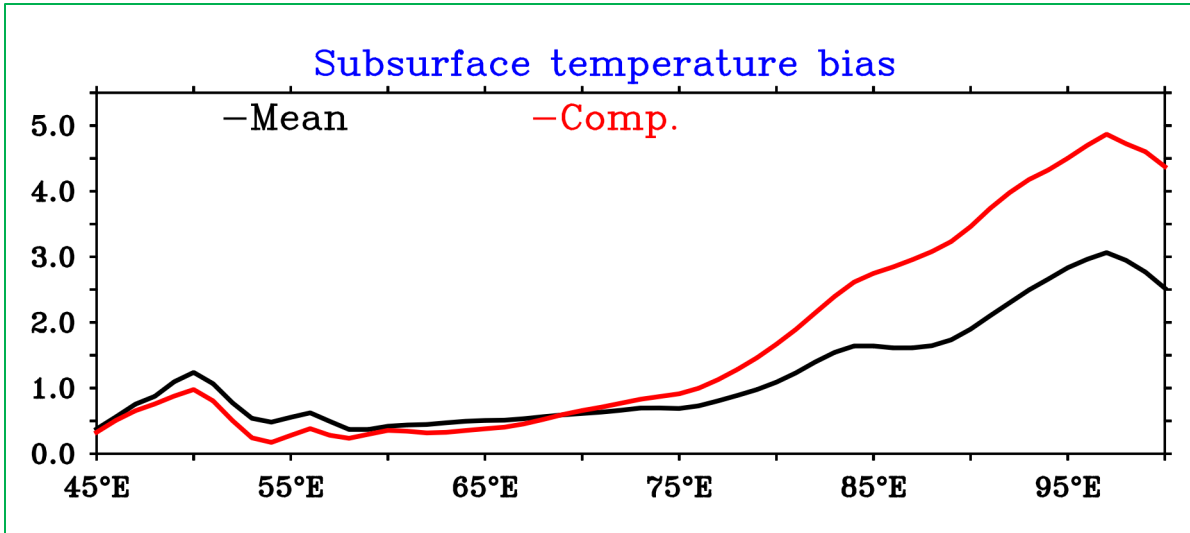

This warm bias is higher than mean bias, highlighting the role of interannual variability in contributing to the mean subsurface bias.

Srinivas et. al. 2018
Climate Dynamics

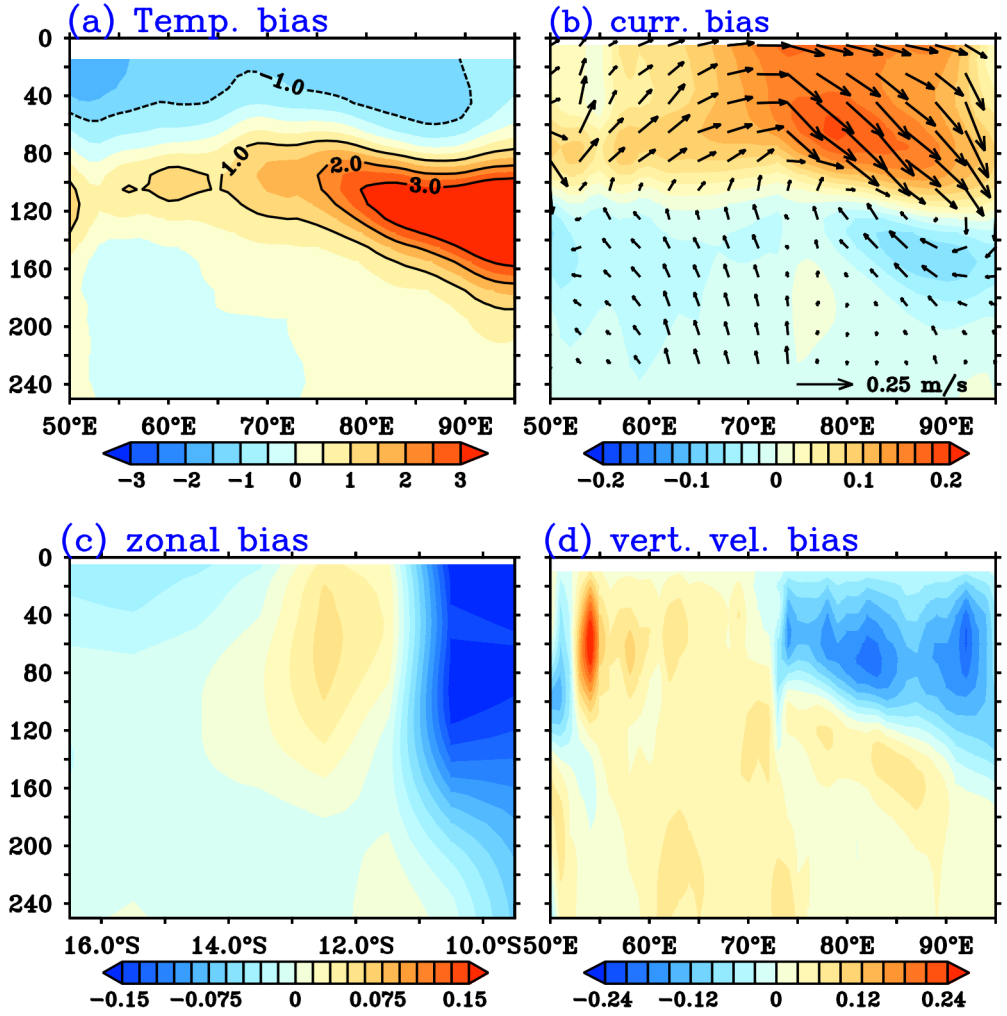

✓Depth-longitude plot of temperature bias shows about 4°C warm bias at 120 – 140 m depth over the EEIO region during strong warm years.

✓Anomalously strong eastward bias in currents up to 120 m depth is evident in strong warm years.

✓ This equatorial current bias supports subsurface warm bias in the EEIO by accumulating warm water and deepening the thermocline.

Bias (JJAS) of upper 250 m depth – longitude plot (averaged over 3°S to 3°N) for composite of strong warm years (a) temperature (shaded and contour; °C), (b) zonal current (shaded; m/s) and zonal and vertical currents (x10^4) (vectors; m/s), (c) depth – latitude plot of zonal current (averaged over 110°E to 115°E) (shaded; m/s) and (d) vertical current (shaded; 10^4 m/s).

To test the impact of EIO winds and current bias on subsurface temperature bias, we have carried out a couple of sensitivity experiments with OGCM by changing surface wind forcing. In Exp-1 composite of strong warm years (ERA-Interim ERA-COMP) surface wind forcing is used to run the ocean model and in Exp-2 similar composite of winds obtained from CFSv2 are used.

OGCM forced by

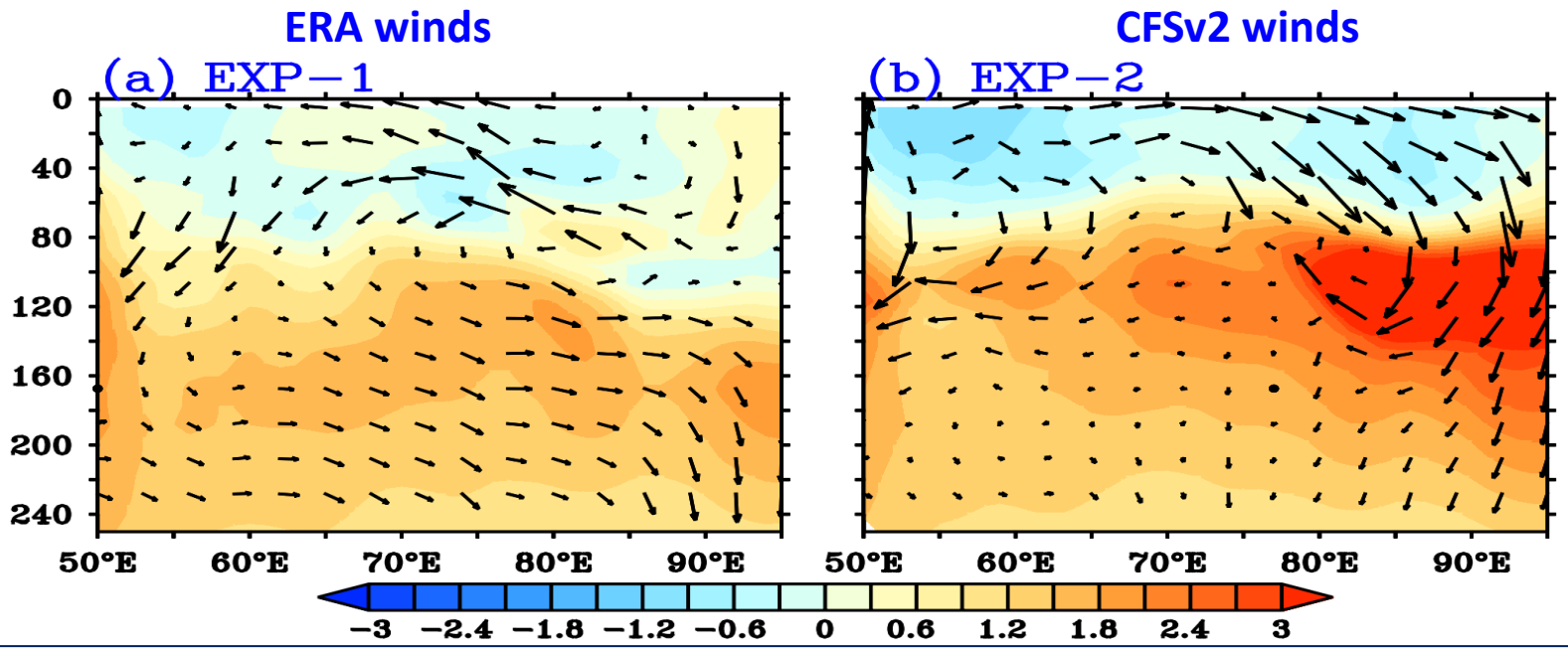

Depth – Longitude plot (JJAS) of upper 250m (average over 5°S -5°N) bias of a) Exp-1 temperature (shaded; °C) and zonal and vertical currents (10^{-4} m/s) (m/s), b) for Exp-2.

SUMMARY

➢The subsurface temperature bias in CFSv2 has been traced.

➢ Strong warm bias associated with interannual events such as La Niña mainly contribute for mean bias in the model. Both coupled model and OGCM simulations support this.

Clim Dyn (2018) 50:1659–1673
DOI 10.1007/s00382-017-3713-y

CrossMark

Association between mean and interannual equatorial Indian Ocean subsurface temperature bias in a coupled model

G. Srinivas[1,2] · Jasti S. Chowdary[1] · C. Gnanaseelan[1] · K. V. S. R. Prasad[2] · Ananya Karmakar[1,3] · Anant Parekh[1]

Received: 8 February 2017 / Accepted: 26 April 2017 / Published online: 3 May 2017
© Springer-Verlag Berlin Heidelberg 2017

ENSO Response

Chowdary et al. 2015, Climate Dynamics

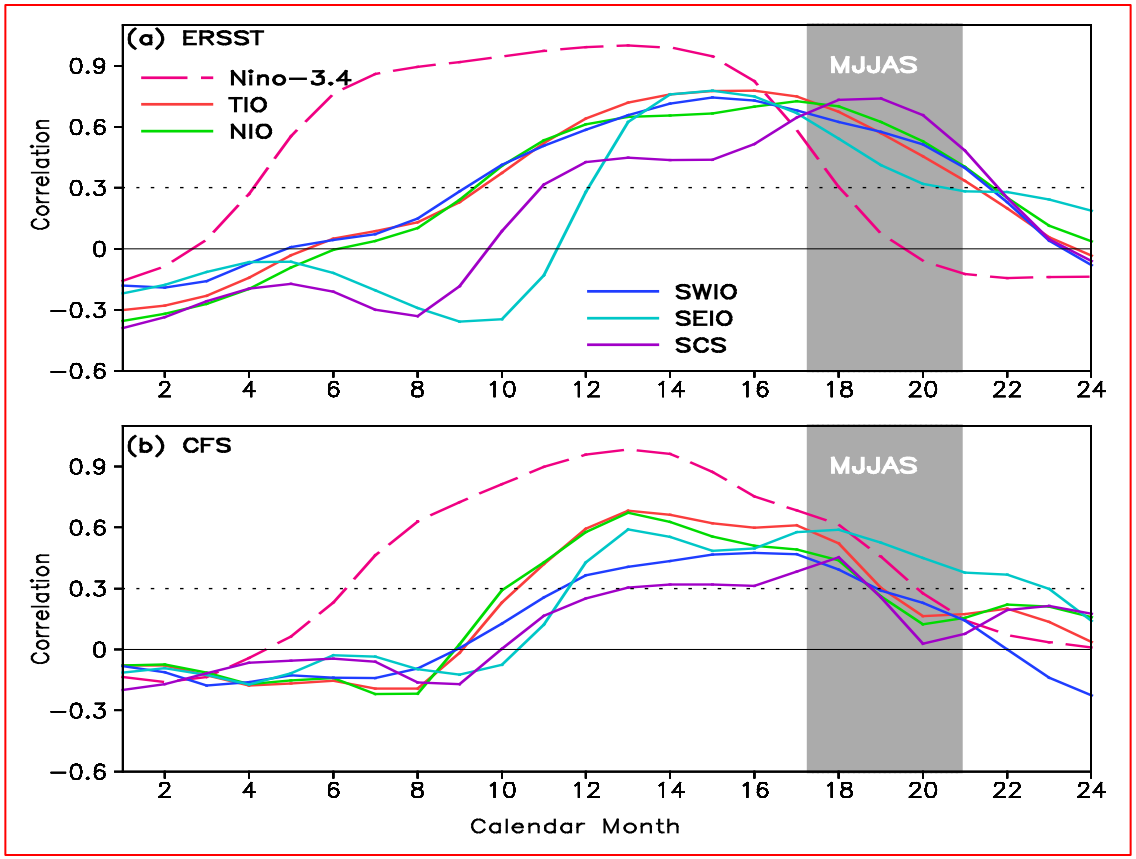

✓The TIO warming induced by El Niño at its peak phase (winter; DJF) and following spring (MAM+1) are well represented in the model.

✓Though El Niño decay is delayed by two months in the model, decay of TIO SST warming is faster than the observations.

DJF Niño-3.4 SST index correlation with the TIO (20°S to 20°N and 40°E to 100°E) NIO (Equator to 20°N and 50°E to 100°E), SWIO (15°S to 5°S and 50°E to 70°E), SEIO (10°S to Equator and 90°E to 110°E) and SCS (4°N to 20°N and 105°E to 120°E) SST anomalies during the El Niño developing and decay year (a) ERSST and (b) CFSv 2-free run. The dashed thick li ne (Magenta) is for the lagged autocorrelation of the Niño-3.4 index with DJF(0/1) values.

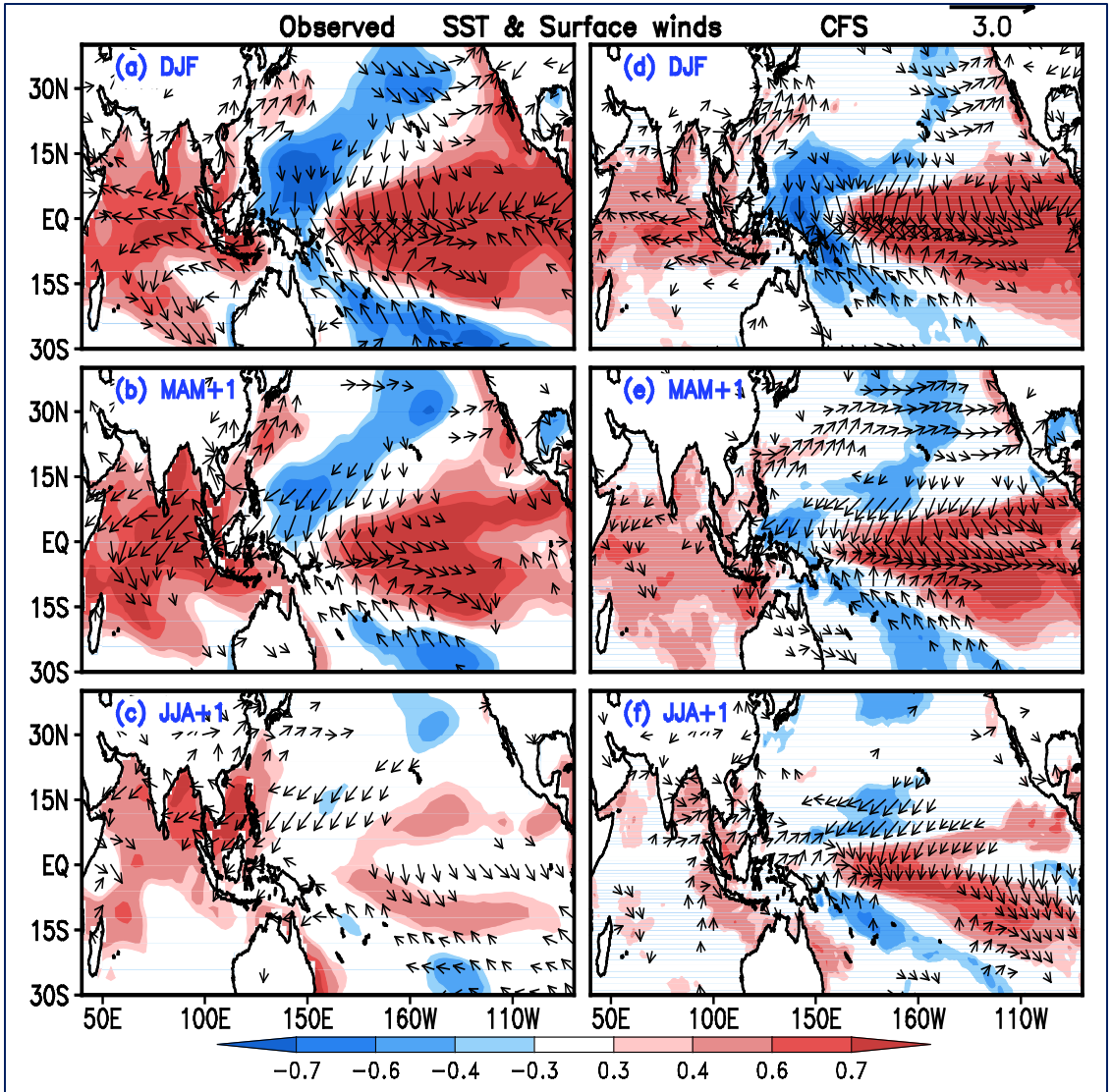

Correlation of SST (shaded) and surface wind anomalies (vectors) from DJF to JJA+1 during decay phase of El Niño with DJF Niño-3.4 SST index for (a-c) observations and (d-f) CFSv2-free run. Displayed signals are significant at 90% confident level.

✓The TIO basin-wide warming induced by El Niño at its peak phase (winter; DJF) and next spring (MAM+1) are reasonably well captured by the model but with weak magnitude.

✓This TIO basin-wide SST warming persists until summer (JJA+1) and exert strong impact on summer monsoon rainfall and circulation as revealed in the observations.

✓However, TIO SST anomalies are very weak in the model during the El Niño decaying summers.

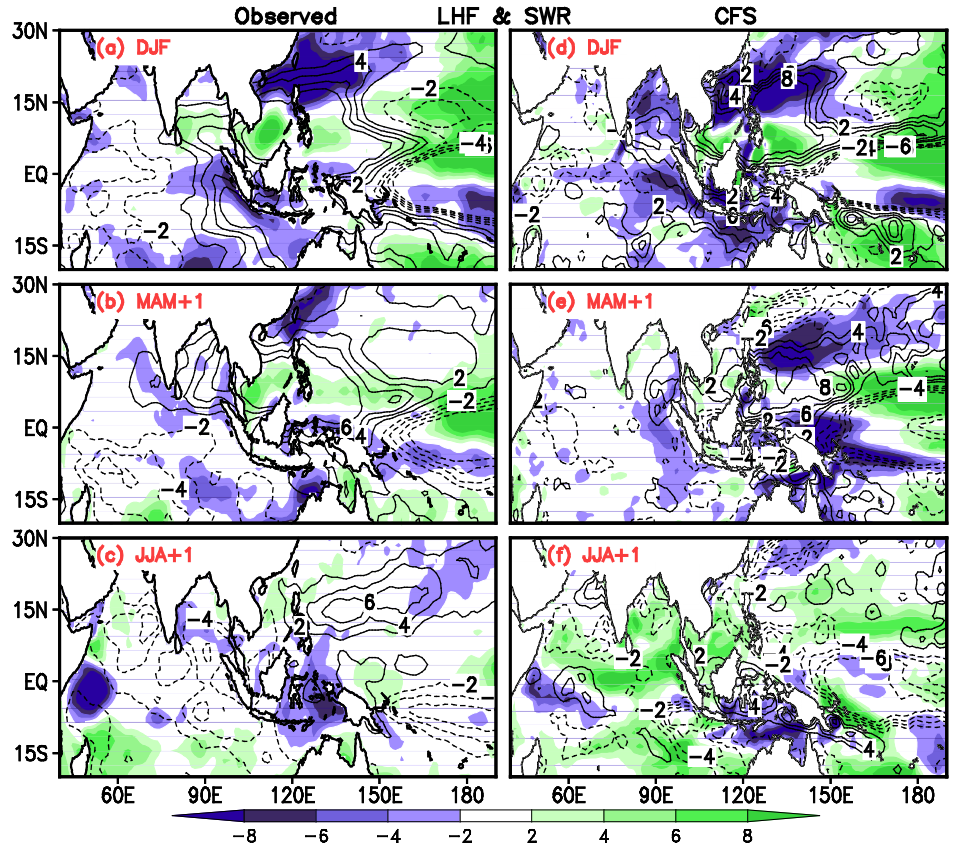

Regression of Latent heat flux (shaded; Wm^{-2}) and Shortwave radiation (contours; Wm^{-2}) from DJF to JJA+1 during decay phase of El Niño upon DJF Niño-3.4 SST index for (a-c) observations and (d-f) CFSv2-free run.

❑Anomalous latent heat loss from ocean and a feeble southern TIO Rossby waves associated with weak wind response to El Niño are mainly accountable for rapid decay of TIO SST warming by mid-summer in the model. This suggests that JJA+1 TIO SST response to El Niño decay phase in the model is poorly represented.

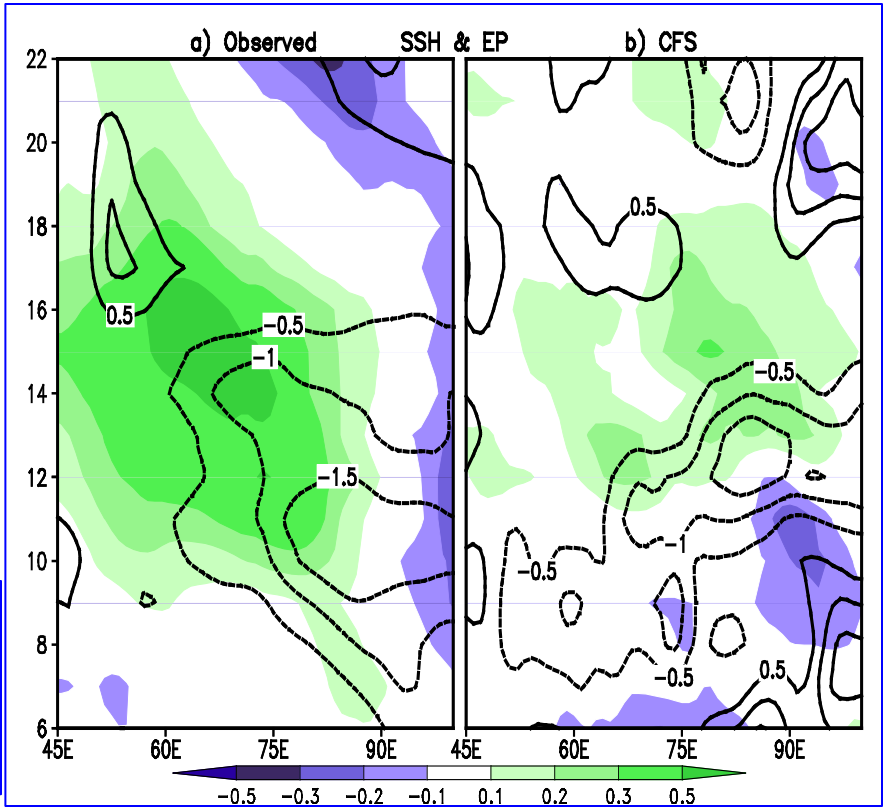

Regression of SSH (shaded, m) and Ekman pumping (contours; 10^{-6} m/s) anomalies averaged over the SIO (from 17°S to 5°S) upon the DJF Niño 3.4 index as a function of calendar month and longitude for (a) observations and (b) CFSv2-free run.

Rashmi et al. 2019, Clim Dyn

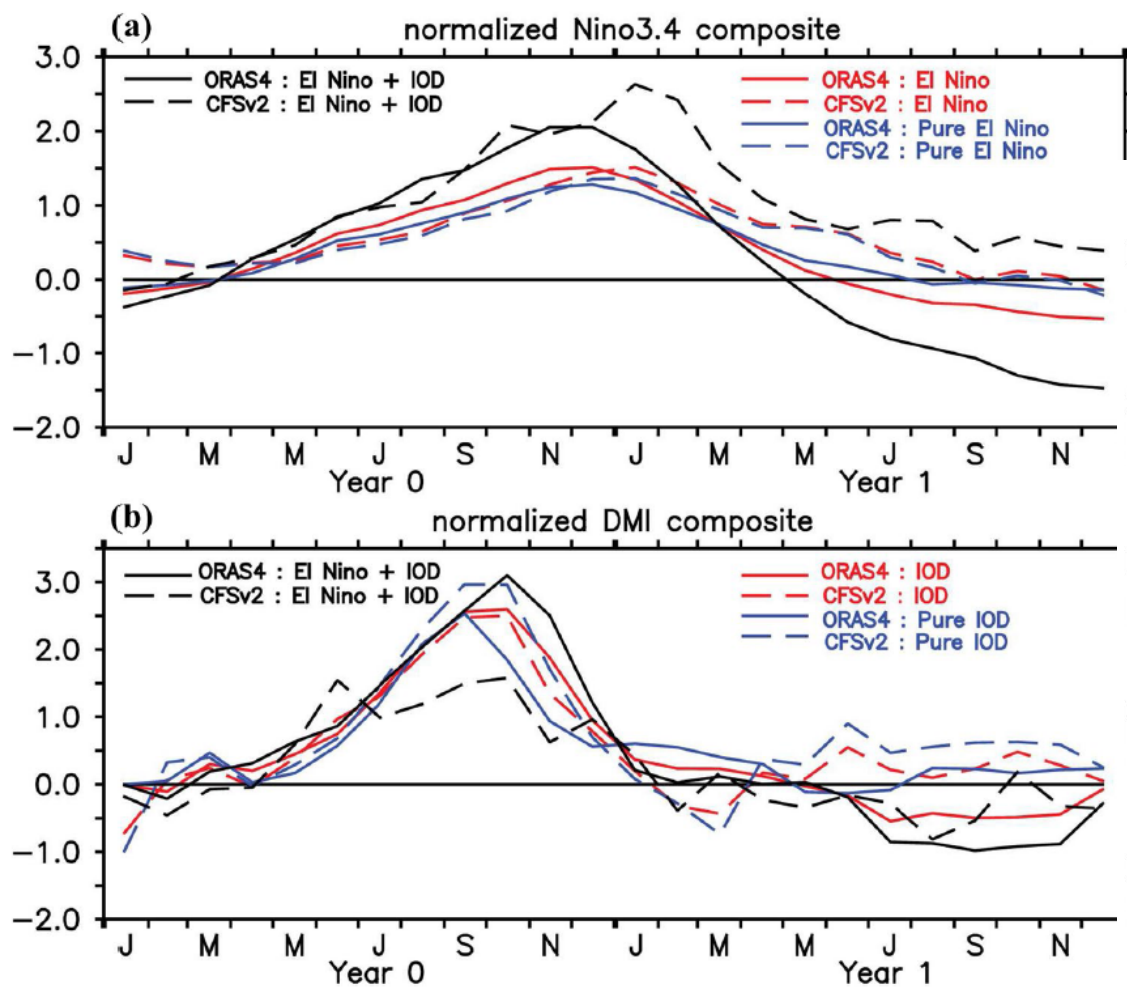

Eq. zonal winds (shaded) and curl (10°S)

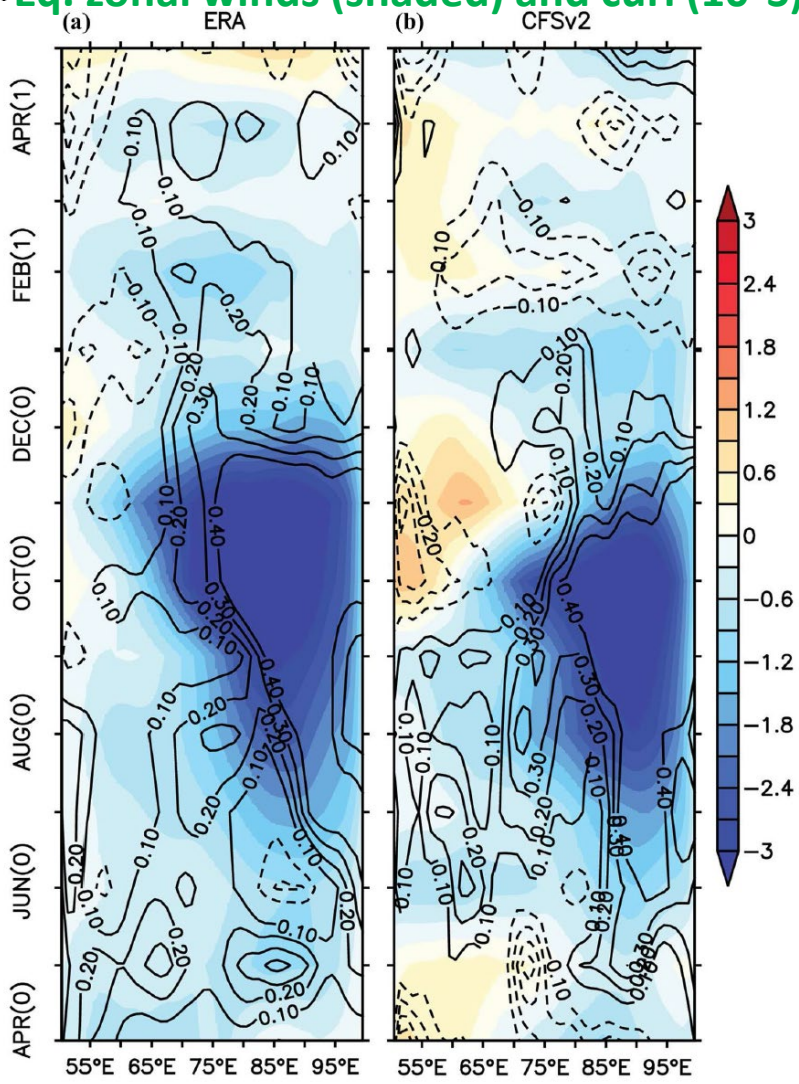

Composite of normalized a Niño3.4 and b DMI indices for a El Niño (red), Pure El Niño (blue) and El Niño, IOD co-occurrence (black) years. b IOD (red), Pure IOD (blue) and El Niño, IOD co-occurrence (black) years. Solid line represents ORSA4 and dash line represents CFSv2

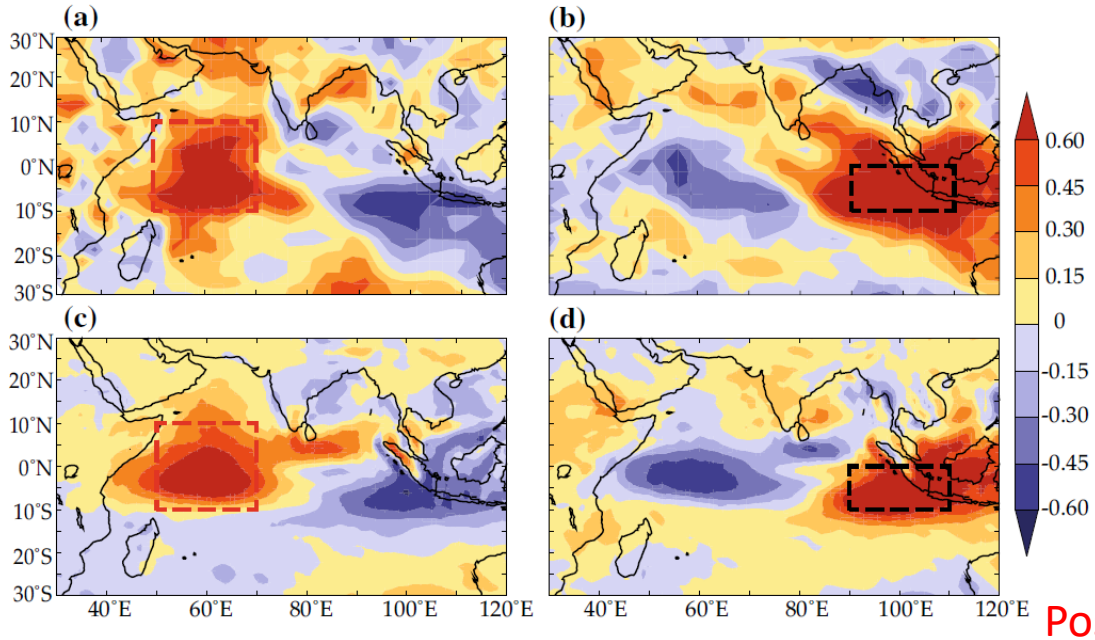

Observed

Model

Correlation with Western Box

Correlation with Eastern Box

Positive EQWIN

Negative EQWIN

Observed

Model

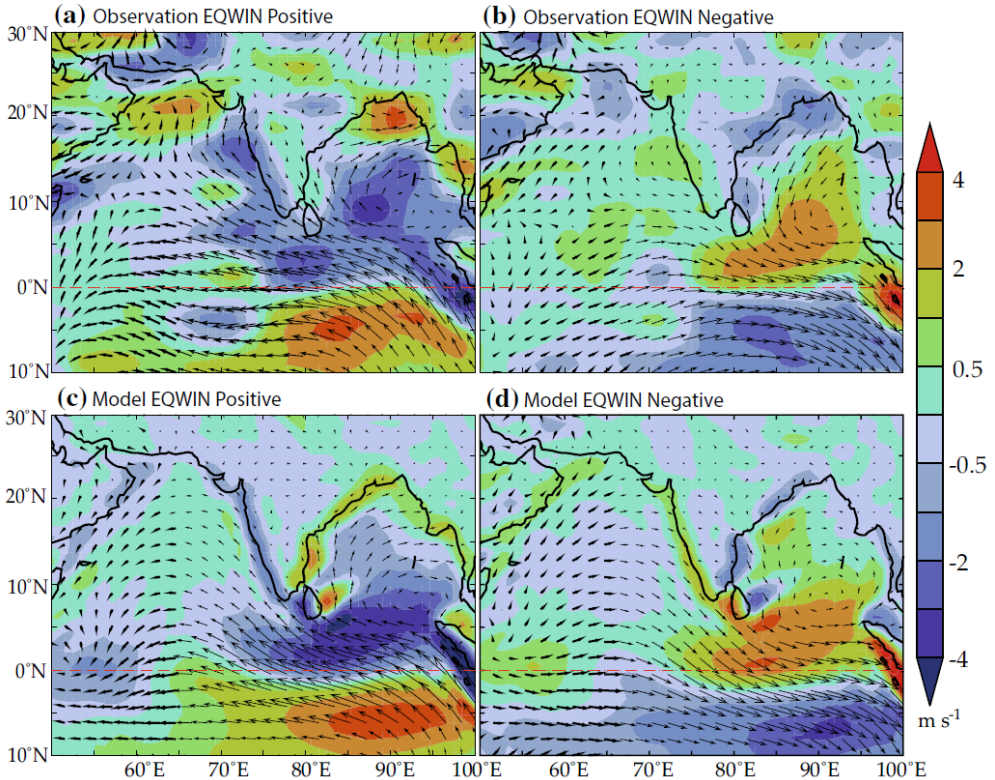

Vishnu et al. Clim Dyn, 2018

Subsurface temperature variability in CFSv2 hindcasts

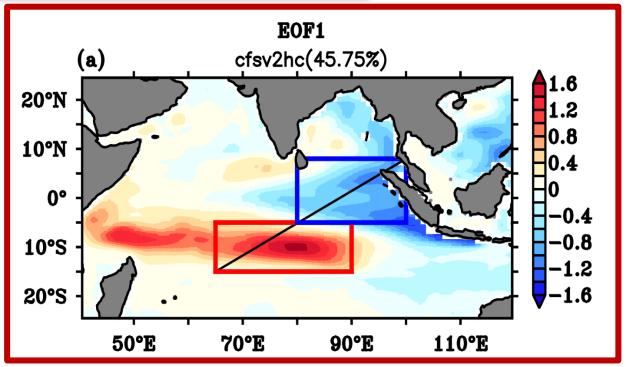

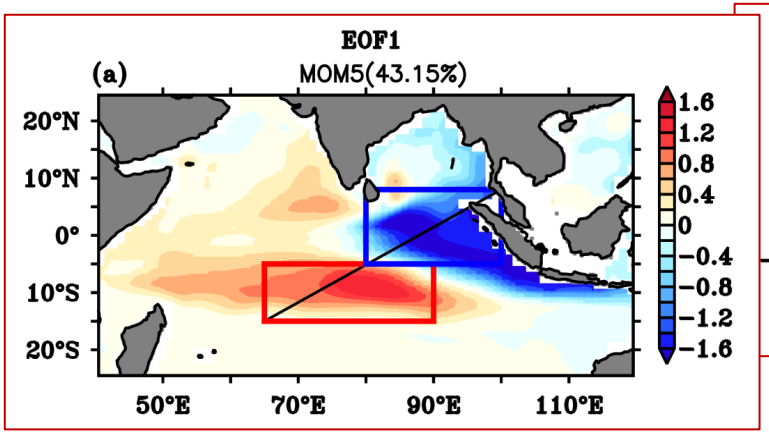

Sayantani & Gnanaseelan, 2015

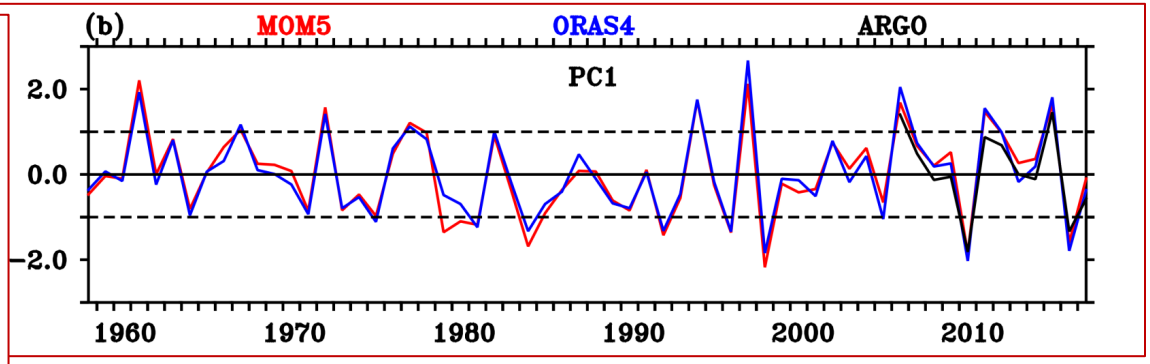

Rashmi et al. 2019

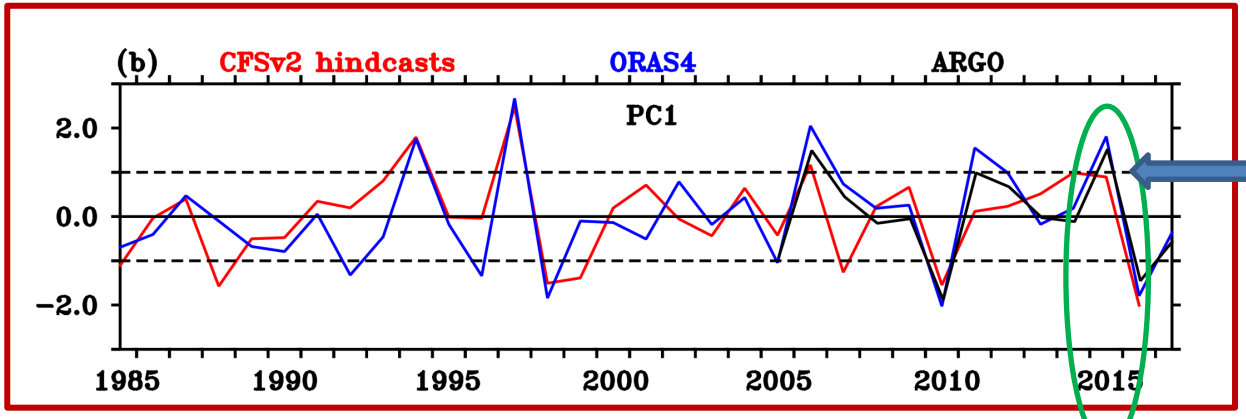

2015 event is not captured by CFSv2 hindcast

Individual and combined Impact of TIO warming and WNP anticyclone using coupled model sensitivity experiments with the 1990 initial conditions

Experiments

- EXP1 -- > WNP convection is suppressed to excite anticyclone
- EXP2 -- > Strong TIO basin-wide warming is imposed
- EXP3 -- > (EXP1+EXP2) Combined influence

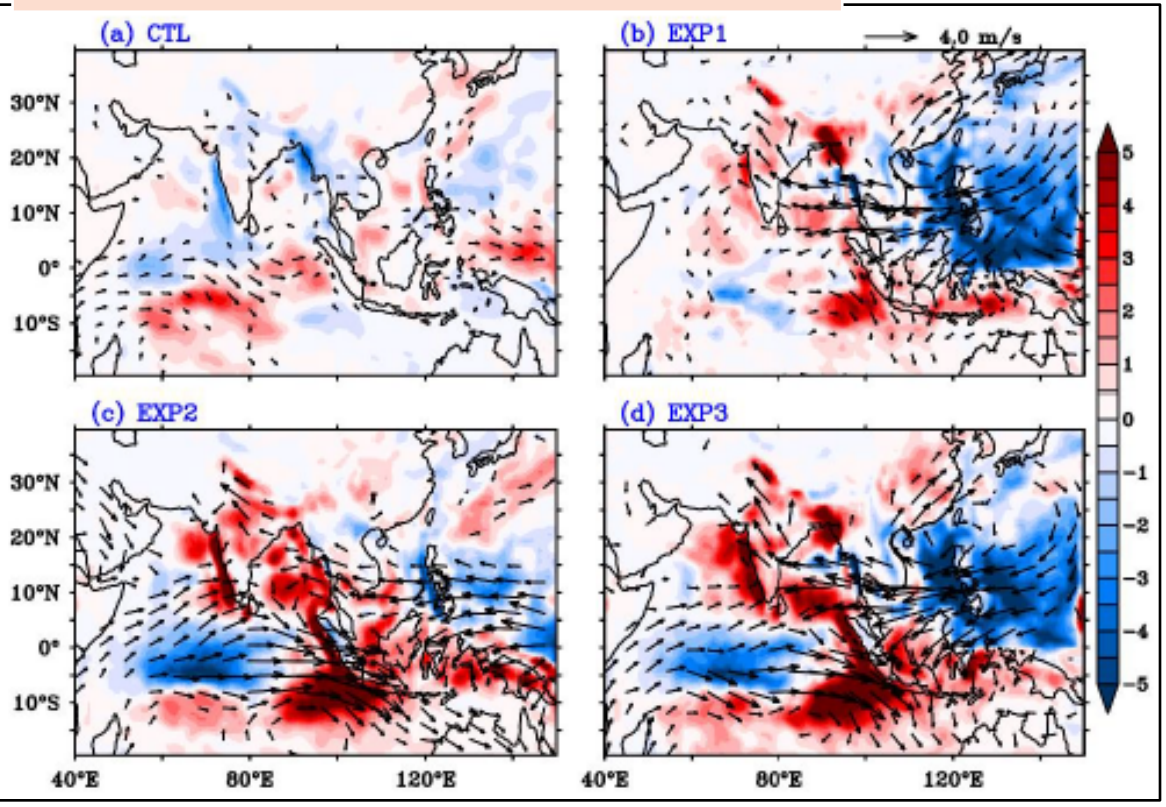

JJA precipitation (shaded; mm/day) and 850hPa winds (vectors; m/s) for (a) CTL (JJA 1990), (b) EXP1, (c) EXP2 and (d) EXP3.

Chowdary et al. (2019), Climate Dynamics

❖ EXP1: AAC and negative precipitation anomalies over WNP region

❖ EXP1 and EXP3 :
Enhanced rainfall over the Sundarbans and Bangladesh region due to
Low level convergence in the northern flank of AAC over these regions

Reduced rainfall (weak) over the east coast of India/monsoon trough
region due to moisture divergence associated with the westward
extension of WNP AAC

❖ Enhanced rainfall over the western Ghats and southern peninsular India are strong in EXP2 as compared to EXP1, suggesting that TIO warming is mainly responsible for this positive rainfall anomalies

⇒ TIO warming contributes to the positive rainfall of about 80%
associated with IPOC mode over the western Ghats-eastern Arabian
Sea region

❖ EXP2 :Low rainfall over the monsoon trough region and high rainfall over the Sundarbans are not well represented, indicating that TIO warming impact is less over these regions (c).

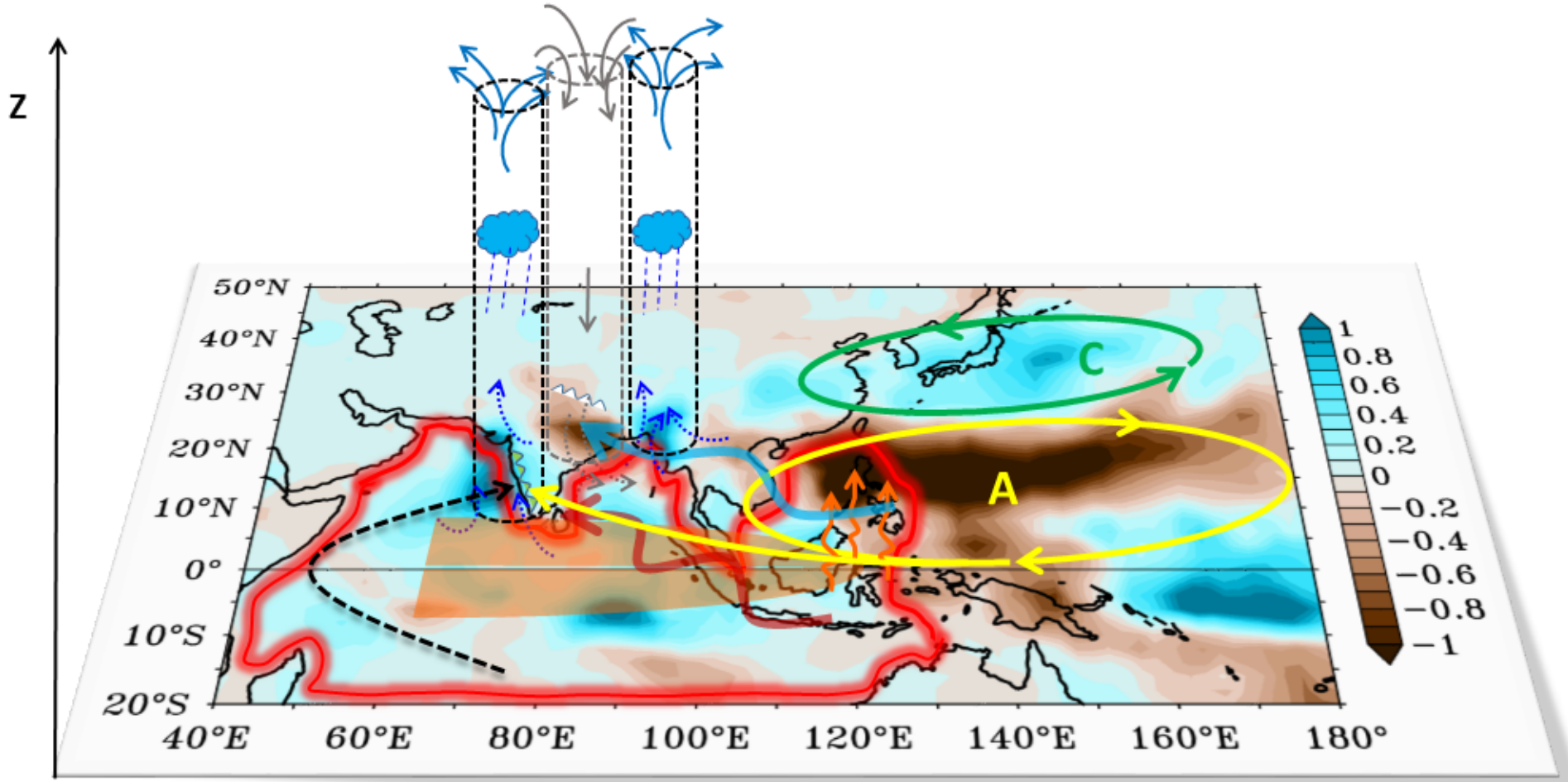
Z
50°N
40°N
30°N
20°N
10°N
0°
10°S
20°S
40°E
60°E
80°E
100°E
120°E
140°E
160°E
180°
C
A
1
0.8
0.6
0.4
0.2
0
−0.2
−0.4
−0.6
−0.8
−1

Indo-Western Pacific Ocean Capacitor mode and South Asian Summer monsoon rainfall

SVD analysis of WNP (0-30°N, 100-160°E) 850hPa vorticity and TIO (20°S–20°N, 40°E-100°E) SST in JJA to extract IPOC mode (50.5% of variance)

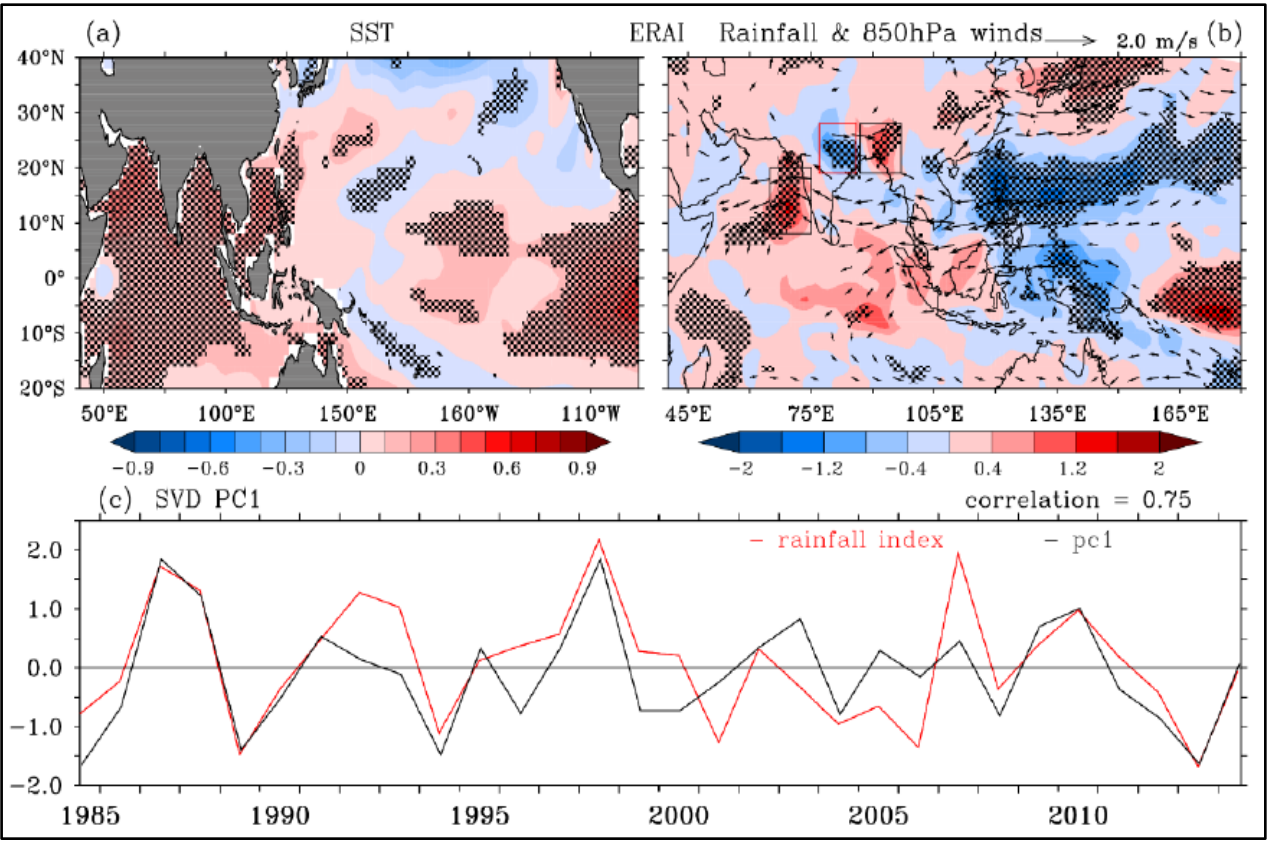

Regression of PC1 upon (a) SST (shaded; °C), (b) Precipitation (shaded; mm/day) and 850hPa winds (vectors; m/s) and (c) Normalized time-series of observed SVD PC1 and rainfall index

Rainfall anomaly index = Box A (+ve) + Box C (+ve) - Box B (-ve)

IPOC mode signals: (a) Anomalous warming over South China Sea, TIO and cooling in the Philippine and Japan Seas, (b) Strong anomalous anticyclonic (AC) circulation over WNP easterlies over NIO and weak north-easterlies over western TIO

IPOC mode impact: (a) Tri-pole rainfall pattern over South Asian region, (b) Significant Corr between PC1 and rainfall index indicates strong relationship between IPOC mode and ISM rainfall

CFSv2

Coupled model hindcast (using May initial condition prepared for 30 years (1985–2014))
Model skills capturing the IPOC mode and its impact on ISMR rainfall

Impact of IPOC mode on ISM rainfall is well captured by model

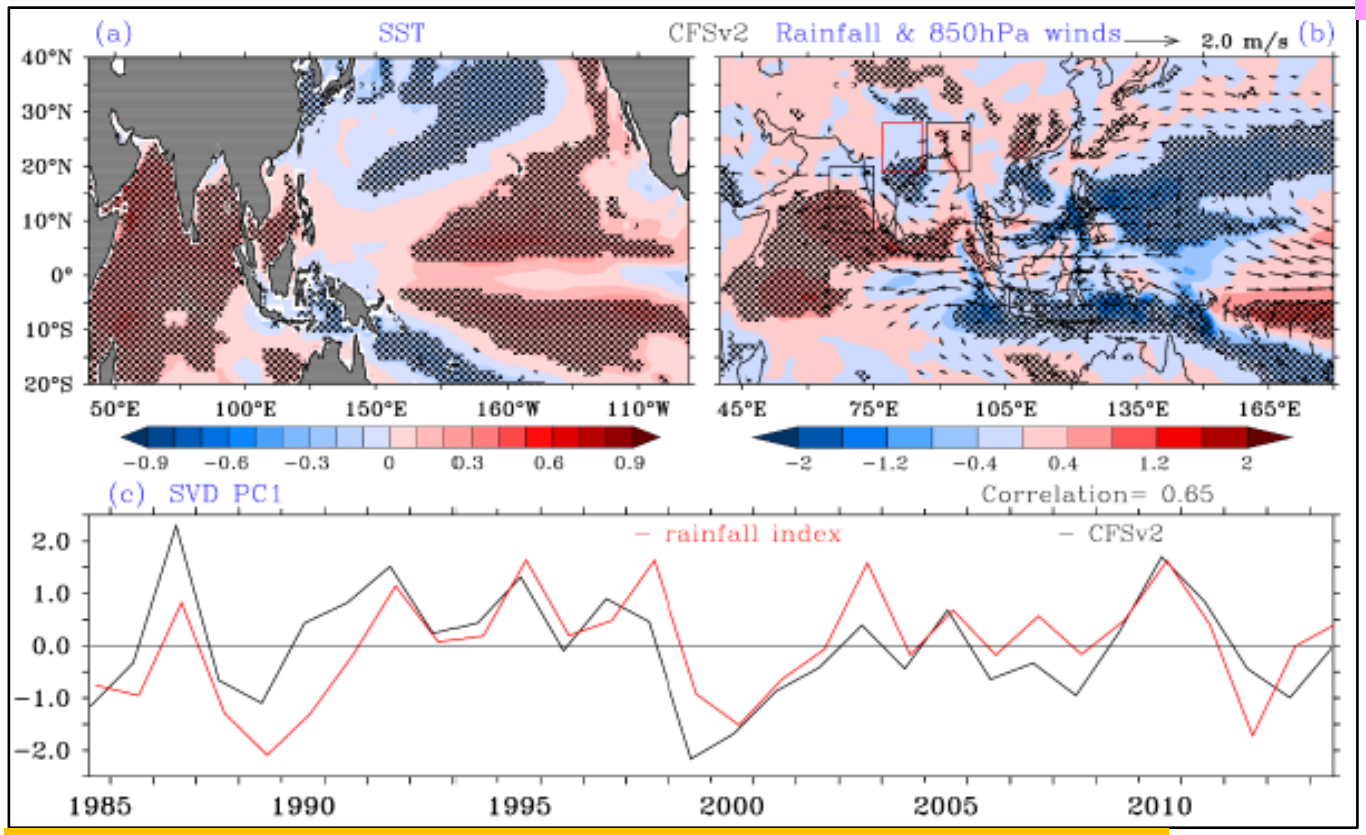

Regression of PC1 upon (a) SST (shaded; °C), (b) Precipitation (shaded; mm/day) and 850hPa winds (vectors; m/s) and (c) Normalized time-series of observed SVD PC1 and rainfall index

Model has good skills in representing the inter-annual variations of the IPOC mode.

Regression of PC1 upon (a) SLP (contours; hPa), Tropospheric Temp (shaded;°C), (b) Vertically integrated moisture transport (vectors; m/s), moisture divergence (mm/day), and (c) 200hPa Velocity Potential (shaded; x106 m3s−1) and Divergent winds (Vectors; s−1).

Observed

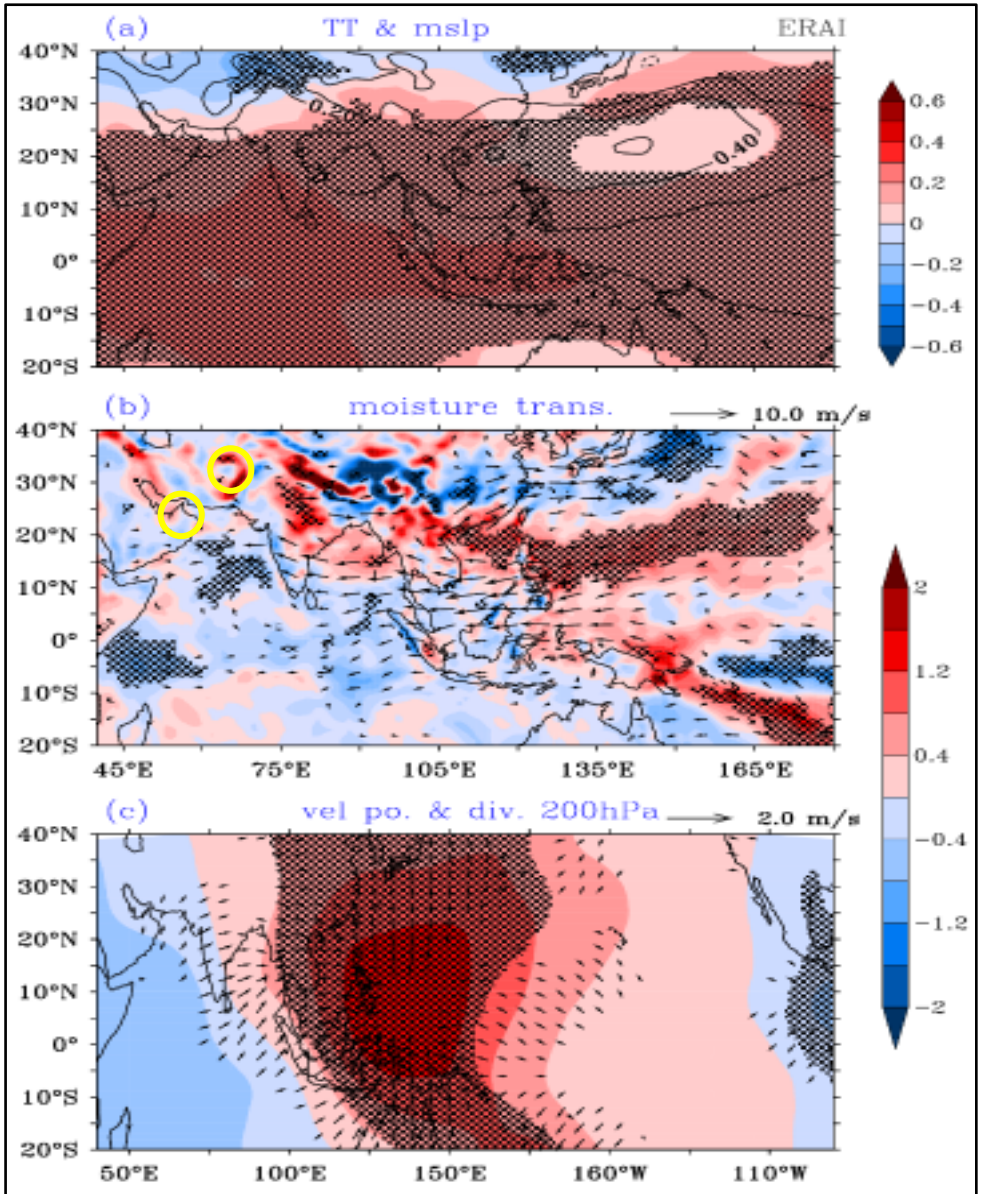

CFSv2

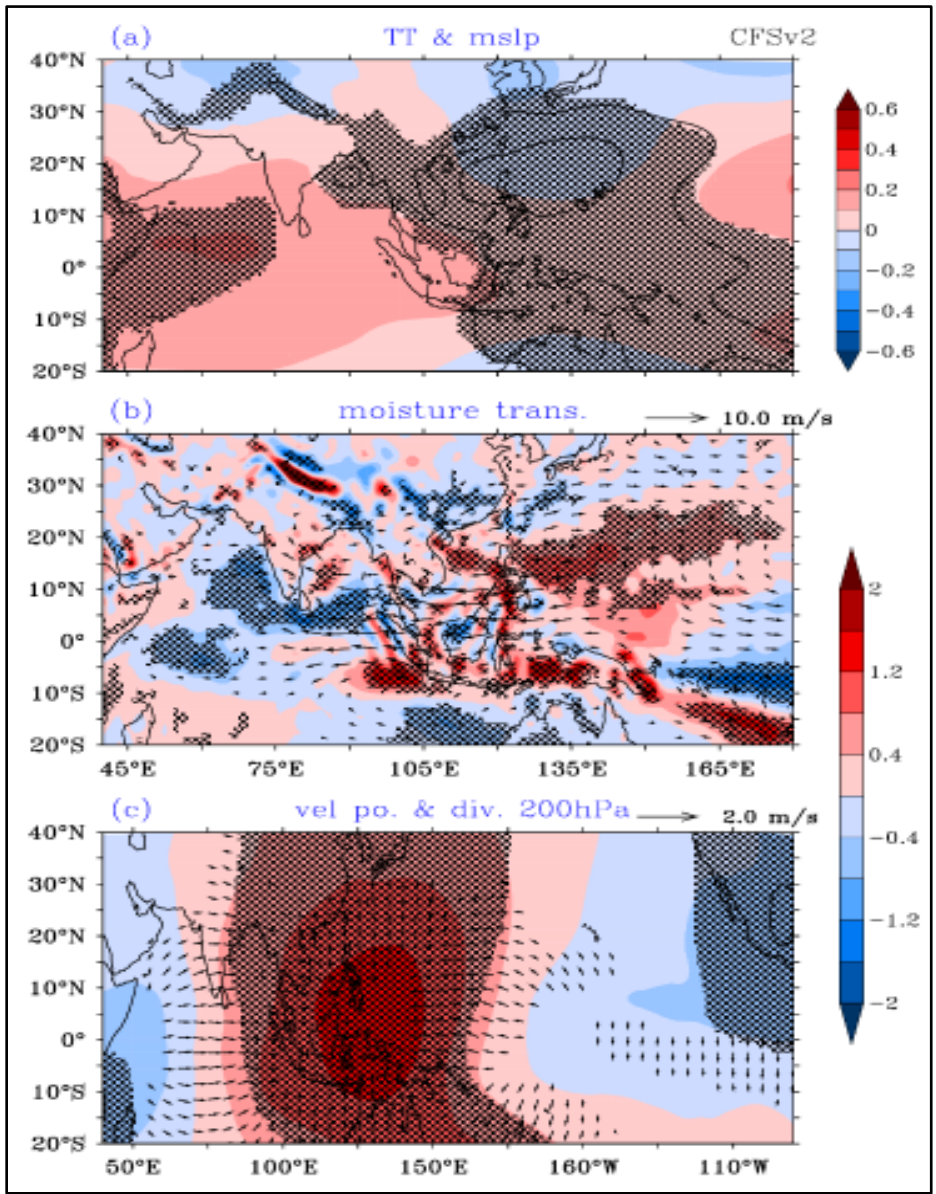

Impact of the Indo-Western Pacific Ocean Capacitor mode on South Asian Summer monsoon rainfall.

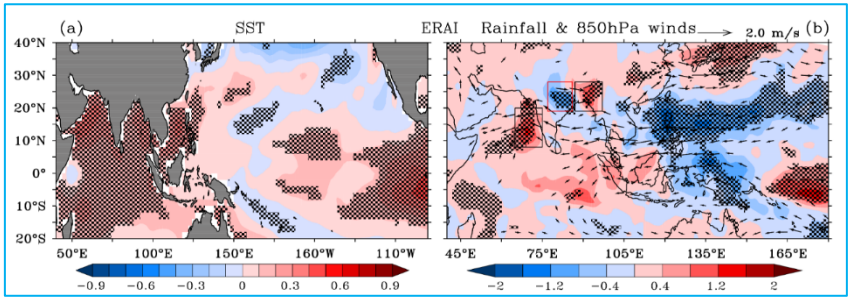

Regression of observed JJA SVD PC1 on the Indo-Pacific region (a) SST (shaded; °C), (b) Precipitation (shaded; mm/day) and 850hPa winds (vectors). Hatched regions are significant at the 90% confidence level.

It is found from the observations that the IPOC mode induces a tripole pattern in precipitation anomalies over the South Asian region. Strong positive precipitation anomalies over some parts of western Ghats and Sundarbans and Bangladesh region separated by negative precipitation anomalies over the monsoon trough region are found to be the main characteristic features closely associated with the IPOC mode. Anomalous western north Pacific (WNP) anticyclone and tropical Indian Ocean (TIO) warming maintain tripole precipitation pattern over South Asia region. Westward propagating atmospheric cold Rossby wave as a response to suppressed convection induced negative rainfall anomalies over the monsoon trough.

IPOC monsoon teleconnection

Schematic diagram showing the factors responsible for changes in ISM rainfall associated with the IPOC mode. Red thick curve represent SST warming over the TIO and SCS regions, Yellow arrows show WNP anticyclone and easterlies over Bay of Bengal (850 hPa) and Green arrows for cyclonic circulation. Low level convergence and upper level divergence and vice-versa (with in the cylinders) associated with convection and subsidence respectively are shown over the South Asian region. Red and blue arrows represent warm and cold Rossby waves.

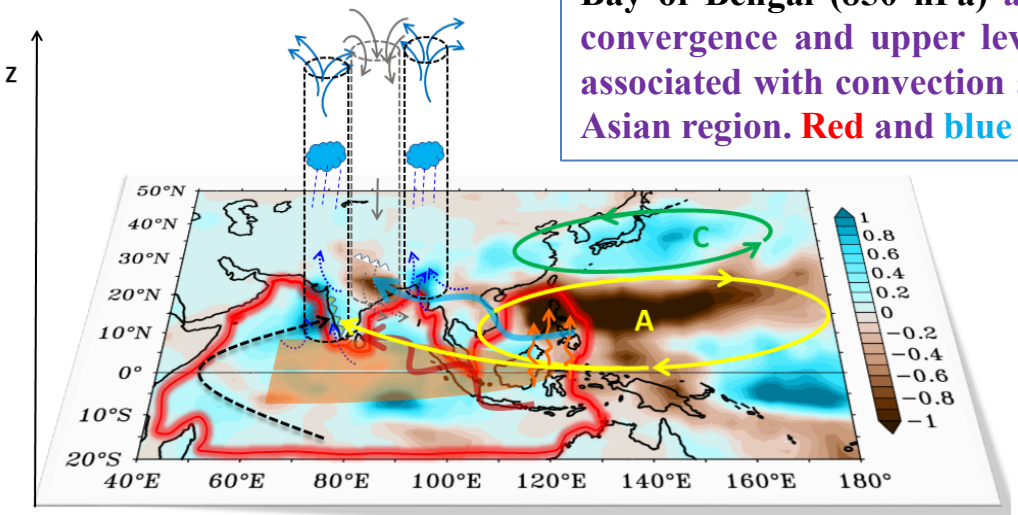

Chowdary et al. (2019), Clim Dyn
Darshana et al. (2019), Clim Dyn

Summary…….

- IPOC mode induces anomalous tri-pole pattern in the precipitation anomalies over ISM region In response to the IPOC mode, presence of strong positive anomalies over eastern Arabian Sea-western Ghats of India and Sundarbans-Bangladesh region and negative precipitation anomalies over the monsoon trough region are noted.
- This tri-pole pattern in rainfall over South Asian region is mainly contributed by anomalous WNP AAC and TIO warming, which are the two components of IPOC mode.

- Coupled model sensitivity experiments shows that TIO warming caused for positive rainfall anomalies over the western Ghats region contributing to about 80% of rainfall associated with the IPOC mode which is due to the enhanced convergence corresponds to local SST warming as represented in EXP2.

- EXP1 shows enhanced rainfall over the Sundarbans and Bangladesh region and reduced rainfall over the monsoon trough region suggesting the contribution (about 75%) of WNP Anticyclone

- IPOC mode can exert strong impact on regional summer rainfall variability over South Asian/Indian land region via TIO warming and WNP anticyclone.

- This study highlights the possible role of the TIO warming and WNP circulation in influencing/predicting South Asian summer rainfall.

Influence of the Pacific-Japan Pattern on Indian summer monsoon rainfall

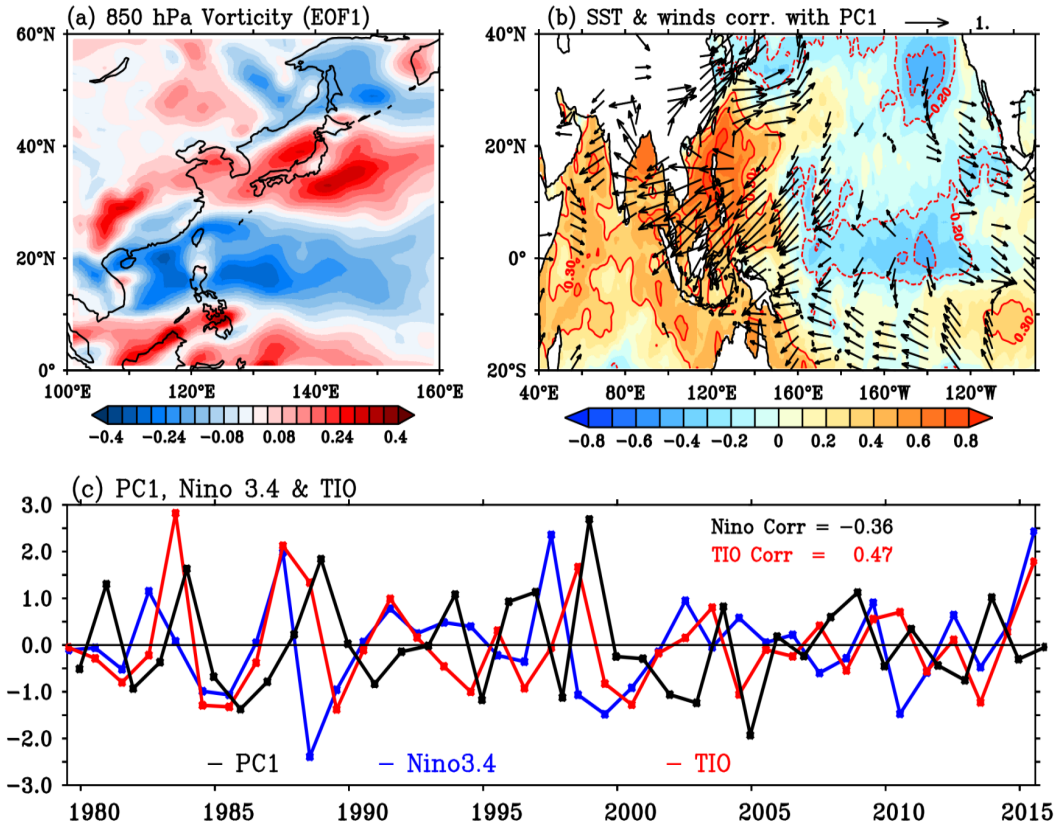

Boreal summer season (JJA): (a) EOF1 of relative vorticity at 850 hPa (shaded), (b) correlation of RV-PC1 with SST (shaded) and surface wind (vectors) anomalies, and c) time series of **RV-PC1 (black line)**, **SST anomalies of Niño 3.4 (blue line)** and **TIO (red line)**. Contours and vectors are significant at 95% confidence level.

Impact of the Pacific-Japan (PJ) pattern on Indian summer monsoon (ISM) rainfall and its possible physical linkages through coupled and uncoupled perspectives.

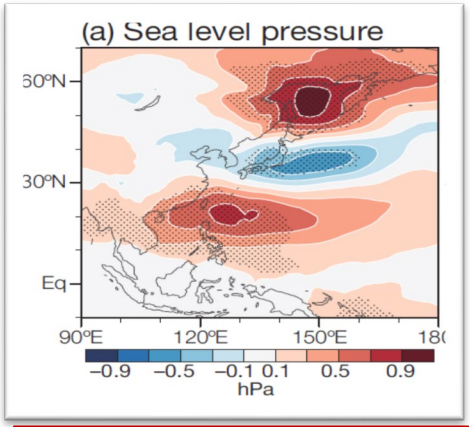

Structure of the PJ pattern

Srinivas et al 2018 – J. Climate

PJ pattern evolved as the leading mode of circulation variability over NWP

Srinivas et al 2018. – J. Climate

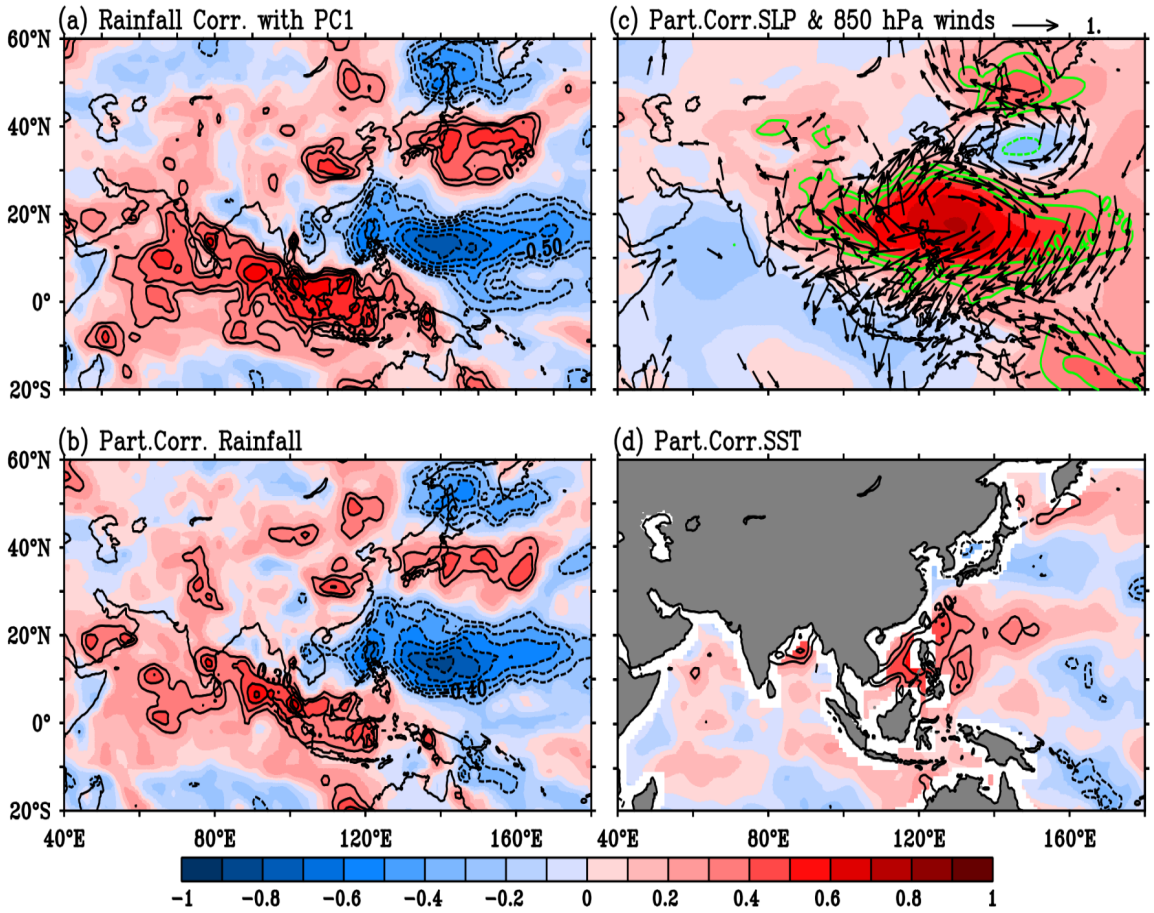

Spatial patterns in boreal summer: (a) raw correlation of RV-PC1 with rainfall (shaded and contour), (b) partial correlation of RV-PC1 with rainfall after removing the influence of Niño 3.4 and TIO indices (shaded and contour), (c) same as in (b) but for MSLP (shaded) and winds at 850 hPa (vectors) and (d) same as in (b) but for SST anomalies. Contours and vectors are significant at 95% confident level.

The partial correlation analysis with the leading principle component revealed that the positive phase of PJ pattern enhances the rainfall over the south and northern parts of India. The northwestward propagating Rossby waves, in response to anomalous convection over the Maritime Continent supported by low level convergence in the southern flank of westward extended tropical NWP anticyclone, increase rainfall over the southern peninsular India.

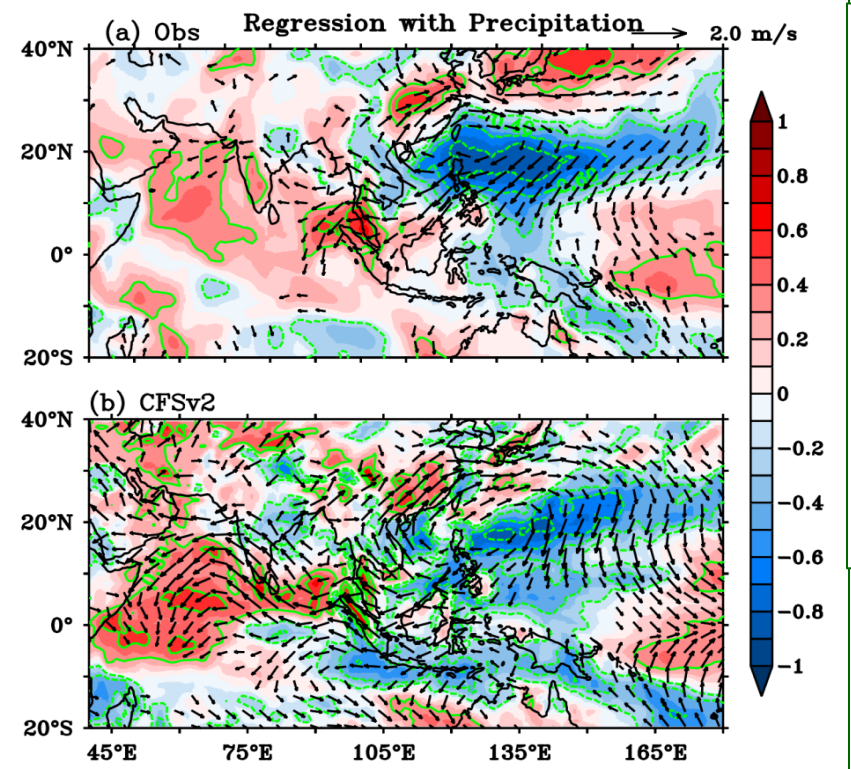

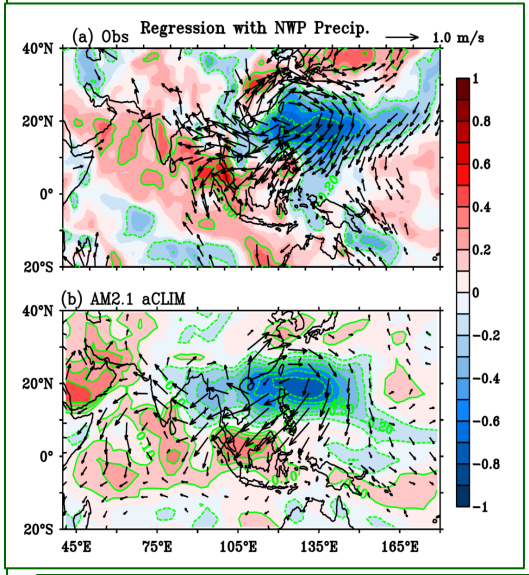

AGCM experiments

Spatial pattern of JJA anomalous precipitation (mm/day) and 850 hPa winds (m/s) for (a) CTL run, (b) EXP run and (c) their difference (EXP minus CTL).

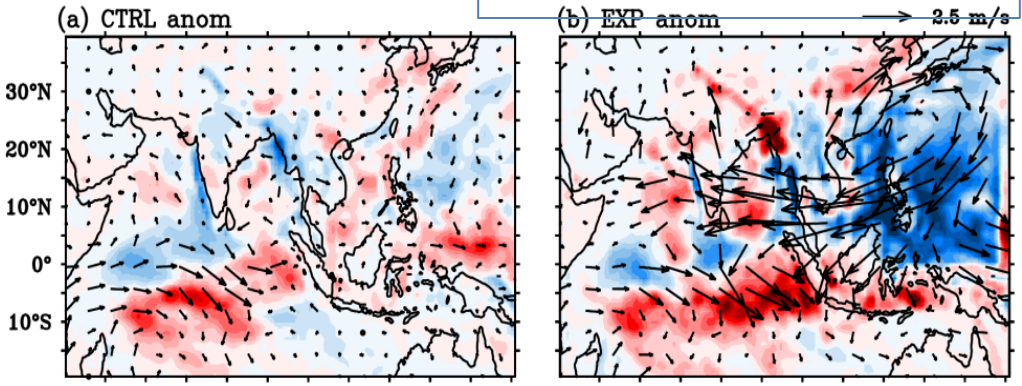

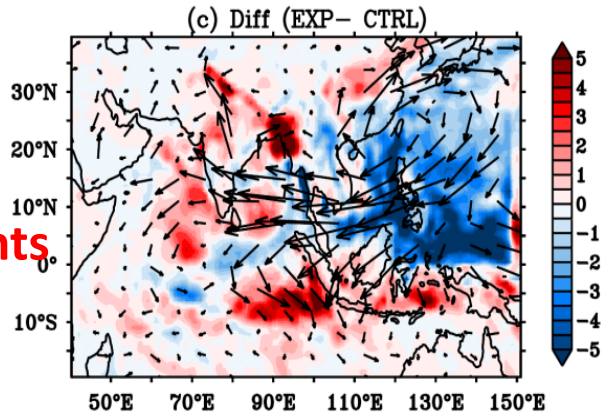

Regression of precipitation averaged over the tropical NWP region (latitude 15 – 25°N and longitude 110 – 150° E) with anomalous precipitation (mm/day) and 850 hPa wind (m/s). Partial regression in observation and in AM 2.1 climatological SST run (top right panels).

CFSv2 coupled Model experiments

Srinivas et al 2018, Journal of Climate

SUMMARY

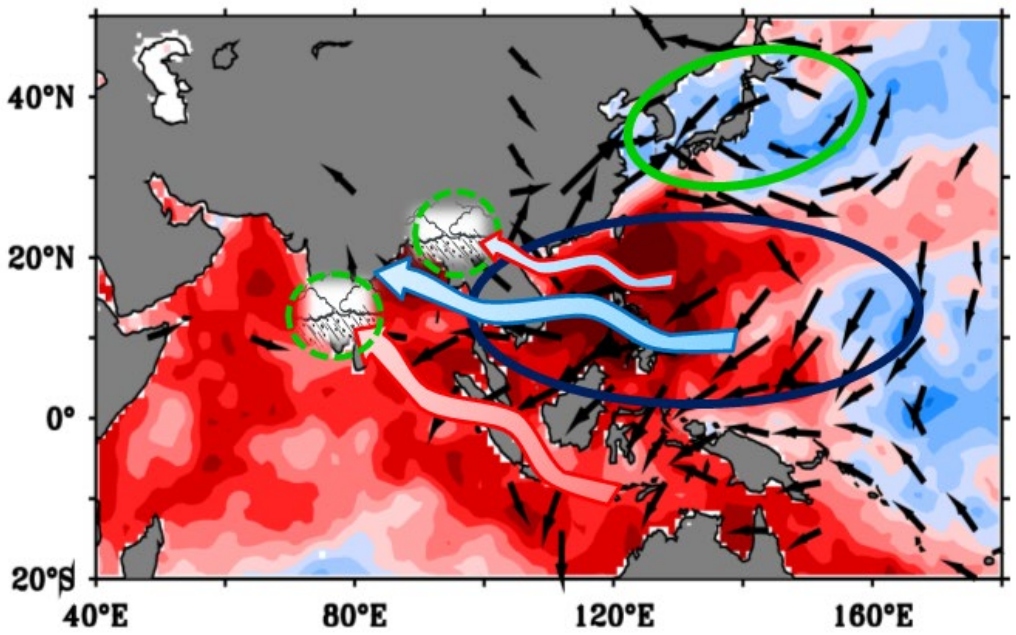

Schematic showing PJ – ISMR teleconnection

Impact of the Pacific-Japan (PJ) pattern on Indian summer monsoon (ISM) rainfall and its possible physical linkages through coupled and uncoupled pathways are explored. *The* northwestward propagating Rossby waves, in response to intensified convection over the Maritime Continent increase rainfall over the southern peninsular India. The relation between the PJ pattern and ISM through NIO is further examined in a coupled model (CFSv2). A PJ like anomalous circulation pattern is generated in a coupled model experiment by imposing negative vorticity through modulating local negative SST anomalies over the tropical NWP region during summer. This result indicates that the PJ mode plays an important role in ISM rainfall variability.

Thank You